NTNU
Norwegian University of
Science and Technology

# Tailoring multifunctional nanoparticles for encapsulation of bio-molecules.

Karthik Raghunathan

Chemical Engineering
Submission date: August 2017
Supervisor: Jens-Petter Andreassen, IKP
Co-supervisor: Sulalit Bandyopadhyay, IKP

Norwegian University of Science and Technology
Department of Chemical Engineering

# Acknowledgement

I would like to thank my supervisor Dr.Jens-Petter Andreassen for accepting me as his student. His guidance, insight and advices helped in completing this project. I could not have had a better advisor.

I would like to thank Dr.Sulalit Bandyopadhyay for his support throughout the project. His knowledge in nanoscience helped me tackle difficult problems and his patience and encouragement allowed me to learn and improve.

I would also like to thank my friends ArunKumar Pannerselvam and Anuvansh Sharma for helping me to finish the project in time. I would also like to thank Greg Rutkowski for the discussions on science, politics and everything.

Finally I thank my family for their love and support.

# Abstract

Nanoparticles(NPs) that can simultaneously perform multiple tasks could be used for sensing, imaging, monitoring, delivering drug among other things. Combining organic and inorganic NPs has been used to synthesize such multifunctional NPs. In such multifunctional NPs, the inorganic NPs can be used for sensing or detecting etc, while polymeric NPs make them stable and help in active targeting or delivering drug. Inorganic NPs like gold(Au) NPs or iron(Fe) NPs posses good sensing, detecting and imaging properties. On the other hand, stimuli responsive polymers such as Poly(N-Isopropylacrylamide) (PNIPAm) and Acrylic Acid (AAc) respond to changes in temperature and pH respectively. Combining these two NPs will result in multifunctional NPs with the properties that are mentioned above.

This work mainly focused on developing new techniques to synthesize polymeric NPs and multifunctional NPs. As part of the study, the physico-chemical properties of these NPs were also analysed. Polymeric NPs were synthesized using PNIPAm and AAc. These polymeric NPs were combined with Au NPs or Fe NPs to synthesize multifunctional NPs. Different sizes, shapes and concentration of inorganic NPs were used to study its effect on the multifunctional NPs

Different sizes and shapes of Au NPs and Fe NPs were synthesized. The smallest NPs were around 46$\pm$4nm while the biggest were 150$\pm$3nm. Two new synthesis techniques were developed to synthesize PNIPAm/AAc polymeric NPs. These were called flashing and impeller methods. These methods were developed to synthesize multifunctional NPs. The polymeric NPs obtained from these methods were compared with polymeric NPs that were synthesized by an already existing method. Their sizes, volumetric collapse efficiencies (VCE) and volume phase transition temperatures (VPTT) were analyzed. The polymeric NPs synthesized by the new method had VCE around 90%. Time based studies were done to understand the growth of these NPs. The flashing and impeller methods were used in *in-situ* synthesis of multifunctional NPs. Flashing method was used to synthesize NPs that showed a VCE of 98.7%. The effect of size, shape and concentration of inorganic NPs were studied. It was found that the size of inorganic NPs was the most important parameter that determines the physico-chemical properties of these multifunctional NPs. The impeller method was used to synthesize multifunctional NPs with Fe NPs which had a VCE of 92%.

The effects of particle sizes, concentrations, shapes and functionalizations on the swelling-collapse properties of the polymeric NPs have been mapped in this study. These make way for a class of multifunctional NPs that can be used for bio-encapsulation without loss in properties of the individual counterparts.

# Table of Contents

# List of Tables

# List of Figures

Chapter 1

# Introduction

Nanoscience has shown that nanoparticles (NPs) can be used in different fields due to their small size and tunable properties.[1, 2] NPs have replaced traditionally used materials in fields like sensing, imaging and drug delivery.[3, 4, 5] Inorganic NPs of Fe and Au are used as contrast agents for magnetic resonance imaging (MRI) and as labels for biosensors respectively.[6, 7] Apart from being efficient, NPs can be used in lower concentrations and achieve similar results.[8] The physico-chemical properties of NPs are also dependent on composition and surface chemistry. Therefore, by altering these properties, NPs can be used for applications that require a specific functionality or outcome and can be used in fields like medicine, catalysis, electronics, sensors and so on. Although individual NPs have many advantages, their real time applications can be limited due to reasons like stability, shelf life, toxicity and reusability. However, these shortcomings can be overcome by imparting multifunctionality to NPs.[8]

Combining different NPs often results in unprecedented physico-chemical properties, giving rise to multifunctional NPs.[9] Such multifunctional NPs, apart fom inheriting properties from their parent NPs, also have other new properties. For example, multifunctional NP synthesized by Liong *et.al.* using iron oxide and silica had magnetic properties from iron oxide, mesoporous structure from silica and it was used for drug delivery. [9]However, one of the major problems in such NPs is deterioration over space and time.[10] This can be averted by surface modification of NPs which can, apart from stabilizing, impart novel properties. With such processes, the application of NPs has broadened its scope in drug delivery, bioimaging, biosensing, monitoring of oil reservoirs, hydrological tracing, antifouling, water treatment. For example, Yang *et al.* showed that magnetic NPs can be combined with polymers and the resulting hybrid can be loaded with target

specific antibody to detect cancer and can simultaneously be used to inhibit the growth of tumor cells.[11] Fig1.1 shows an example of one such NP that has multiple functionalities.

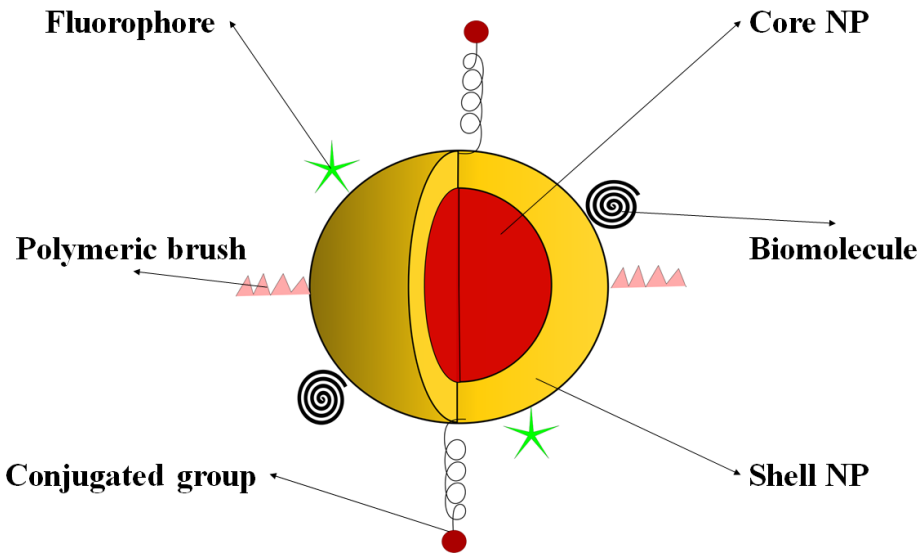


**Figure 1.1:** Schematic representation of multifunctional NPs. [8]

One of the most common methods to introduce multifunctionality is by combining NPs. A number of different shapes and morphologies can be obtained while combining NPs; these include core-shell NPs, Janus particles, alloys and dumbbell structure and other anisotropic shapes. [12, 13] Core-shell NPs are widely researched due their desirable properties and the ease with which these can be synthesized.[14] Based on the constituting materials, these core-shell multifunctional NPs can be classified into the following categories

- Inorganic based multifunctional NPs
- Polymeric based multifunctional NPs
- Hybrid multifunctional NPs

An illustration of these NPs is shown in Fig1.2.

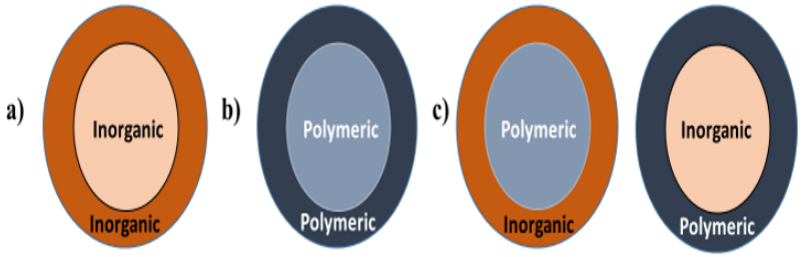


**Figure 1.2:** Schematic representation of different types of core-shell NPs.

## 1.1 Synthesis of multifunctional NPs

The need to find new types of multifunctional NPs has led to the development of a number of techniques to synthesize them. Some of these techniques are discussed in this section.

### 1.1.1 Solution based reduction of metallic precursor

In this process, one type of NP is grown on same or different NP. An example of NP in aqueous phase being grown on another inorganic material was developed at Ugelstad laboratory. In this process, Fe NPs were stabilized with sodium citrate and a gold precursor was added to the reaction mixture to produce Fe@Au core-shell multifunctional NPs. [15]

### 1.1.2 Reverse Micellar Template

In this technique, micelles from two different solutions combine and act as reactors to synthesize NPs. These micelles come in to contact due to Brownian motion, often resulting in coalescence. One of these micelles will contain a metallic precursor, while the other will have a reducing agent. As the micelles coalesce, the metallic precursor is reduced to form NPs.[16] Fig1.3 demonstrates the reverse micellar process to form a NPs. Core-shell multifunctional NPs of Fe@Au and Ni@Au have also been synthesized using this method, the core is first formed, followed by the shell.[17, 18]

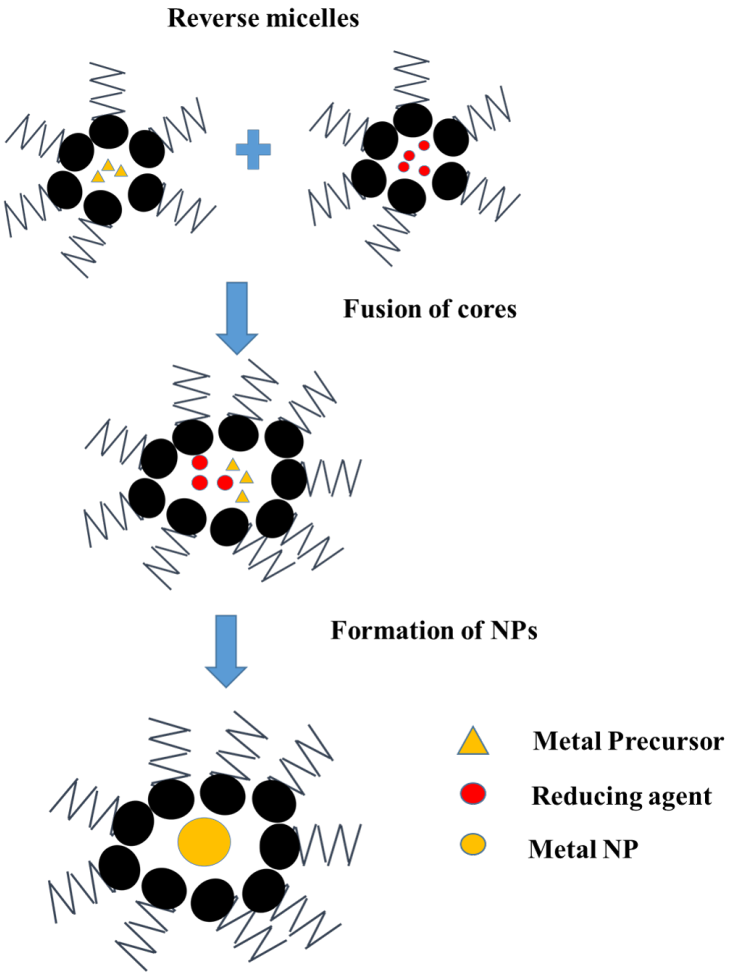


**Figure 1.3:** Adapted schematic representation of reverse micellar process.[14]

### 1.1.3 Dispersion Method

This method is preferred when polymeric NPs are synthesized from preformed polymers, as shown in Fig1.4. One of the common techniques is nanoprecipitation, also called solvent displacement. This is based on the principle of displacement of semipolar solvent from lipophilic solution followed by deposition of polymers.[19] The diffusion of the solvent causes a decrease in interfacial tension, leading to formation of small droplets. Lince *et al.* showed that the overall size of such polymeric NPs depends on the rate of nucleation, growth and aggregation and the monodispersity depends on the time taken for nucleation and growth.[20]

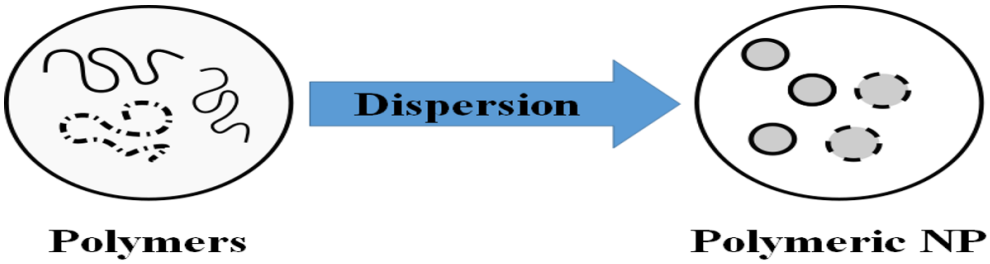


**Figure 1.4:** Schematic representation of synthesis of polymeric NPs.

### 1.1.4 *In situ* growth

In this technique, hybrid NPs are formed, *in situ*, by mixing the inorganic and polymeric precursors required for growth. Based on the type of precursor used, this can be classified as

- *In situ* growth of inorganic NPs in polymer
- *In situ* polymerization on inorganic NPs

#### *In situ* growth of NPs in polymer

The precursors required to form the NPs are mixed with the polymers and the unwanted species are removed after formation of NPs. Techniques such as reduction using chemicals, photoreduction and thermal decomposition can be used to synthesize the NPs. [21, 22] Eisa *et al.* used silver nitrate in a matrix of polyvinyl alcohol- polyvinyl pyridine to get multifunctional NPs.[23] The Ag NPs were easily integrated with the polymers. There are also procedures where the polymeric NPs and inorganic NPs are grown simultaneously. In this technique the polymerization happens as a result of transfer of electrons from the inorganic NPs.[24] Therefore, dispersion of NPs in reaction mixture plays a key role in getting uniform multifunctional NPs.

#### *In situ* Polymerization

The inorganic NPs are dispersed in monomers and polymerized using polymerization techniques like bulk or co-precipitation[25], resulting in formation of multifunctional NPs where the inorganic NPs are in a matrix of polymers. A simple

method of ultrasonication was suggested by Park *et al.*, where Fe NPs were dispersed in epoxy resin.[26] However, stability was an issue and the Fe NPs agglomerated over time.

## 1.2 Functionalization of multifunctional NPs

Functionalization is the process of altering, adding or replacing functional groups on the surface of the NPs to impart stability and/or unique surface properties. Similar to synthesis, functionalization can also be done *In situ* or*post situ*. Functionalizing NPs also plays an important factor when using it for desired application; for example, Medarva *et al.* loaded dye with magnetic NPs for imaging, siRNA delivery and killing tumor. [27]
Some of the functionalization methods are given below and illustrated in Fig1.5

- Ligand exchange and ligand modification
- Passivation of Surface
- Grafting of synthetic polymers
- Chemical treatment of surface
- Functionalization with cloaking polymer like PEG
- Functionalization with biomolecules.
- Functionalization with fluorophores, radioactive materials

The above mentioned functionalization techniques are explained through a series of examples in the following section. These examples include synthesis and functionalization of different types of multifunctional NPs.

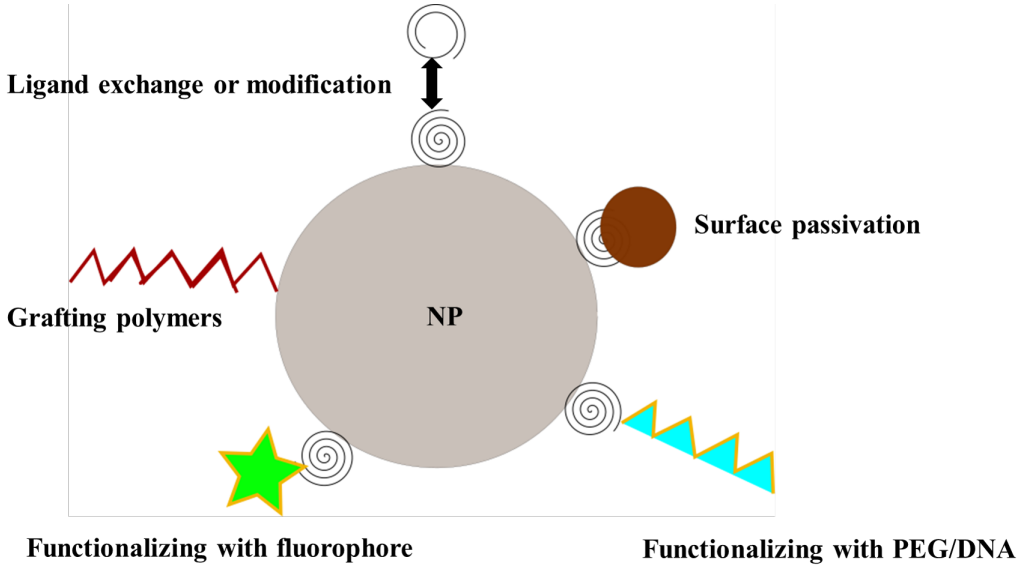


**Figure 1.5:** Functionalization of NPs.

## 1.3 Review on multifunctional NPs

### 1.3.1 Inorganic multifunctional NPs

Combining individual inorganic NPs or functionalizing NPs increases the possible application of the resulting multifunctional NPs. Fe NPs, commonly used for imaging, can also be used for sensing when combined with Au NPs. One of the procedures to obtain inorganic core-shell NPs is by growing the shell layers atop the metallic core. In such NPs, relative thickness between the core and shell plays an important role in determining their physio-chemical properties.[28]

Yoon *et al.* used magnetic NPs to separate living cells by a process called magnetic motor effect.[29] Cobalt ferrite NPs, synthesized by co-precipitation method, were used as the base material. These NPs, soluble in inorganic solvent were functionalized with polyvinylpyrrolione. Functionalization or modification of surface determines how NPs react with their environment, ultimately affecting their overall physico-chemical properties. In this case, it was reported that functionalization helped to improve the overall stability of the NPs. These NPs were then coated with a layer of silica. This process is similar to polymerization reaction; monomeric Trimethoxysilane(TEOS) was added to the NP solution along with an initiator. In such processes, the thickness of shell can be altered by varying the

amount of NPs and coating material.

In order to track the movement of NPs, an organic dye was used to functionalize these NPs, thereby imparting fluorescent property. One of the most widely used methods to impart fluorescence property to the NPs is by functionalizing via ligand modification or chemical treatment of the surface. TEOS, used for coating, was treated with the dye isothiocyanate. This dye is difficult to photo bleach and can easily be studied under confocal scanning laser microscopy (CSLM). The dye forms a covalent bond with the coupling agent used in the coating process. [30, 31]These NPs were further functionalized by polyethelyene glycol(PEG), structure of which is shown in Fig1.6.

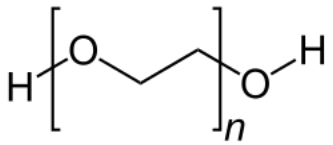


**Figure 1.6:** Schematic representation of PEG.

PEG has the ability to dissolve in a number of solvents, is inert, bio compatibile and non-toxic. When functionalized with PEG, the NPs repel each other due to steric hindrance provided by the hydrated layer in PEG.[32] PEG has also been reported to help phase transfer among semiconducting NPs.[33]NPs with PEG often have stealth properties that are advantageous when using severe conditions where the NPs need to be protected from the external environment.[34]

PEGylation of core-shell magnetic NPs synthesized by Yoon *et al.* allows the NPs to be used for cellular interaction. These NPs were readily internalized by the tumor cells suspended in a solution and the cells responded to an external magnetic field, as shown in Fig.1.7. The organic dye in the NP was used to track the movement of the cells. Such response to external stimuli can be harnessed to impart more functionality to these NPs and can be used in drug delivery.

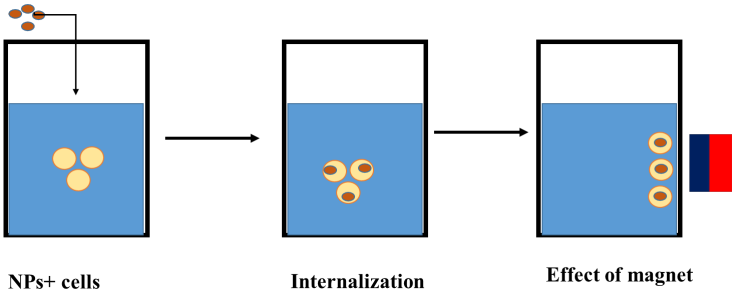


**Figure 1.7:** Magnetic Motor effect observed in cells. [29]

Another widely used category of NPs is Au NPs, they are extensively used for their size and shape dependent optical properties.[35, 36, 37] This ability makes them suitable for optical imaging and photo thermal application. Such Au NPs were modified and were used by You *et al.* for photo thermal, along with drug delivery applications. The photo thermal property was used via thermal ablation of the tumor. [38]

Au shells were grown on top of cobalt(Co) NPs and this acted as a sacrificial template. The difference in redox potential between these metals leads to reduction of Au at the cost of oxidation of Co. Such growth mechanisms where the template is lost after the shell is grown can also be seen in synthesis of hollow silver NPs. [39]

The resulting NPs were conjugated using PEG followed by Doxorubicin, an anti-cancer drug. The type of conjugation of chemicals is one of the most common methods to include multiple functionality to NPs. This process is based on covalent bond or electrostatic attraction between functional groups in these molecules. In order to track the release of drug, the NPs were radiolabeled with $64CuCl_2$, also via conjugation. These conjugations were achieved by chemically treating the surface of NPs.

Chemically treating the surface of NPs can increase their dispersion in a liquid phase and its interaction with other substances. Often, aqueous NPs have carboxylic groups and other molecules can be conjugated with them. For example, Fe NPs form a strong complex with mercaptosuccinic acid fand can be used for cellular uptake.[40] Another example of chemical treatment is reaction with chemicals like alpha cyclodextrin. NPs treated with alpha cyclodextrin behave differently depending on pH; at acidic conditions it has a negative charge and it has positive charge in basic condition. [41]

The radiolabeling technique allowed You *et al.* to track the efficiency of drug release *in vivo* by calculating the radioactivity of samples obtained from animal specimens under study. The radio labeled NPs were injected into mice and the radioactivity was calculated. The NPs stayed in blood stream for extended periods of time and were monitored using a positron emission tomograpy (PET) scans, as shown in Fig.1.8.

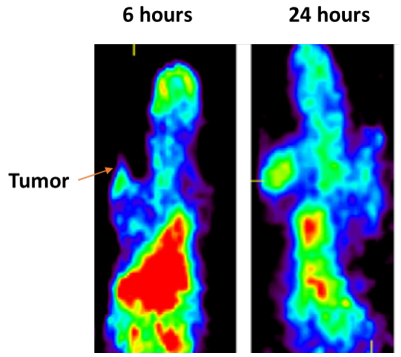


**Figure 1.8:** PET scan of mice injected with NPs. [38]

An accumulation of NPs in the tumour was observed, evident from the PET scans. When non PEGylated NPs were used for *in vivo* study, they were immediately rejected, this reiterated the importance of PEG when used in tough physiological environment. It was also noticed that there was a prolonged release of DOX from NPs making it suitable for controlled release.
A complimentary *in vitro* study was also done and the drug loaded NPs were internalized by cancer cells. On irradiation with Near Infra-Red light(NIR) for, there was an increase in temperature only in the region of cells that had NPs. Such property can be used for treatments that require thermal ablation. These examples highlight the importance of surface treatment and its impact on functionality of NPs.

### 1.3.2 Polymeric multifunctional NPs

The surface chemistry of polymers, which can be easily modified to introduce new properties, along with the ability to control the size and stability of polymeric NPs makes them an ideal candidate for biological and bio-medical applications.[42] These NPs are sensitive to changes in physio-chemical environments; different

polymers respond to different stimuli, combining them will give multifunctional NPs that can respond to multiple stimuli simultaneously.

Leobandund *et al.* synthesized NPs with poly(N-isopropylacrylamide), poly-(ethylene glycol) 400 dimethacrylate, and poly(ethylene glycol)1000 methacrylate, using dispersion method. These NPs were able to respond to temperature, had the ability to deliver drug and were biologically compatible.[43] PNIPAm responds to temperate and delivers drug, other monomers help in shielding the NP from the environment.

The response to temperature was observed by a collapse in size. Heskins *et al.* suggested that the observed change is entropy driven and solvent-polymer and polymer-polymer interactions play a crucial rule for such behaviors.[44, 45] The presence of hydrophobic and hydrophilic components help the collapsing process by expelling water. This is achieved as a result of increase in hydrophobic interactions between polymer-polymer due to loss of hydrogen bonds at high temperature.

The expelling of water is due to phase separation as a result of this interactions. The temperature at which this phase separation occurs is called lower critical solution temperature (LCST). Below the LCST, the polymers are hydrated and an aggregation behavior is observed above LCST. A similar property can be observed in hybrid NPs or cross-linked polymeric NPs where the NPs collapse at higher temperature. This is called Volume Phase Transition Temperature (VPTT)

With the knowledge of LCST of various monomeric units used, Leobandund *et al.* studied the effect of concentration of monomers and the reaction time involved. The NPs were synthesized by using free radical polymerization with Ammonium persulphate as initiator at 85°C, which is above the LCST of all the monomers used in the reaction. As the LCST of NIPAm is less, it will collapse first, resulting in a core shell structure with NIPAm at core.

It was suggested that at 85°C, the collapsed monomers will start to polymerize and the free radical helps them to grow until a certain length beyond which these polymers precipitate to form nuclei. The formed nuclei grow either by capturing other growing oligoradicals or by aggregating with other nuclei. This is called precipitation polymerization and is illustrated in Fig1.9

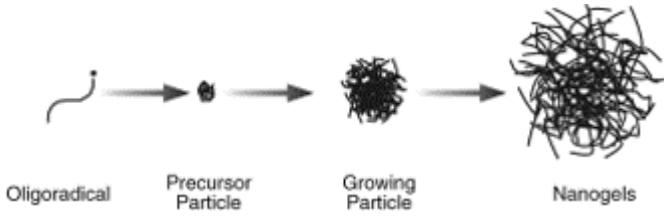


**Figure 1.9:** Schematic representation of precipitation polymerization.[45]

Polymeric NPs, due to their response to stimuli, can be used to functionalize with a cargo and release it when triggered and are extensively researched as an alternative for traditional drug delivery. The interfacial activity between polymers can be used to load cargo molecules. A single step process was suggested in which the polymer and desired cargo are dissolved in organic solvent and emulsified in an aqueous solution.[46] The ligand and amphiphilic co-polymer are introduced in the system and they react with the polymer at the interface. The organic solvent is then evaporated, giving a dispersion of polymeric NPs. This method is called interfacial activity assisted surface functionalization, and was first used to load biotin and folic acid in to polylactide-polyethylene glycol NPs.[46]

Alternatively, if the cargo has a reactive functional group, a simple charge and functional group based functionalization was suggested by William *et al.* to conjugate peptide to the amine group present in polymeric NPs.[47] The process involves treating of polymers followed by interaction with peptides by shaking them together. The conjugation involved is simple, robust, efficient and can be used in many systems.

The polymeric core-shell NPs synthesized by Soppimath*et al.* were used to target cancer cells and deliver a highly hydrophobic anti-cancer drug doxorubicin.[48] The NPs were synthesized from radical copolymerization of N-isopropylacrylamide, N,N-dimethylacrylamide and 10-undecanoic acid. Radical copolymerization helps to produce NPs with narrow size distribution range.

These NPs were chemically treated with folic acid to actively target the cells that overexpress folate. This was achieved by ligand modification of the amine groups resulting in self-assembly to form a core-shell shape as discussed in the previous section with the folic acid in shell. Cholesterol was grafted to the polymer using the hydrophobic part of the NPs. The formed NPs showed a swkkng-collapse response to pH and temperature. DOX was then loaded and the effective uptake of NPs by the cytoplasm and nucleus and its cytotoxicity was studied. The bare DOX, NPs with and without cholesterol and folate were compared, the NPs

functionalized with cholesterol and folate had better binding of DOX along with efficient release of it in response to external stimuli.

### 1.3.3 Hybrid multifunctional NPs

One of the commonly synthesized multifunctional inorganic NPs is Fe@Au core-shell structure. One of the main problems while synthesizing this lies in controlling the shell thickness. Sulalit *et al.* suggested a simple coating process with Fe NPs as seeds.[15] Fe NPs, synthesized by thermal decomposition, were functionalized by citrate followed by addition of a Au precursor,as shown in Fig.1.10. Citrate acts as a capping agent for the NPs and also helps in reducing $Au^{3+}$ to metallic gold, which was coated on to the surface of Fe. The shell thickness was controlled by varying the concentration of gold precursor used. It was suggested that similar protocol can be used for coating noble metals on to heterogeneous nucleation sites.

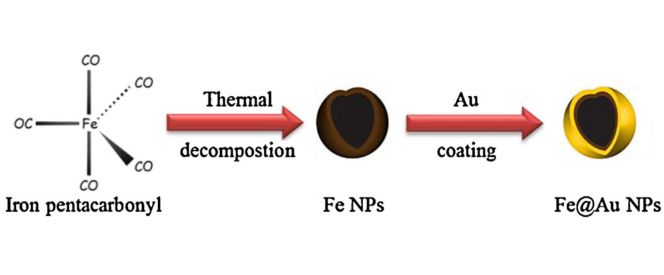


**Figure 1.10:** Schematic representation of synthesis of Fe@Au NP.[49]

These NPs were then coated with stimuli responsive polymeric shells. Polymeric shells can also be coated on to inorganic NPs by grafting technique. A fully grown polymer can be grafted *post situ* or *in situ*. This is a type of functionalization of surface that enhances chemical functionality and surface topology. There are two methods to graft a polymer on the surface,

- Grafting to method - Here, the polymer is attached to an appropriate surface. Using this technique, PNIPAm copolymer was synthesized by radical polymerization and silica was added to it, resulting in PNIPAm coated silica NPs.[50].
- Grafting from method - Instead of polymer, the initiator or one of the other molecules involved in the reaction is grafted on to the surface and the polymer grows on top of it. An alternate method is by grafting polymers on to the surface of NPs using chemical bonding. Here, Au NPs were modified with mercaptododecane and a co-polymer is grafted on to the surface

through Diles Alder reaction between the polymer and modified NP, resulting in hybrid multifunctional NPs.[51]

The as synthesized Fe@Au NPs by Sulalit*et al.* were coated with PNIPAm/AAc *post situ.* The polymeric NPs were synthesized by free radical polymerization and the NPs are formed by precipitation polymerization. These polymers respond to temperature and pH, resulting in hybrid NPs that have optical and imaging properties from Au and Fe respectively along with stimuli responsive properties from the polymeric shells. However, when combining two different kinds of smart nanomaterials, the emergent nanomaterial loses potential in its desired applicability. Additionally, the synthesized NPs did not collapse at high temperature, a key property of the constituent polymer. Instead there was an increase in size at elevated temperature.[15]

An alternative method, *in situ* method, was used in which the Fe@Au NPs were added along with the monomers. This hybrid NP showed swelling-collapse behavior similar to stand alone polymeric NP. The synthesized hybrid multifunctional NPs showed a VPTT of 39°C.[15] The synthesized NPs were further loaded with protein Cytochrome C and its release kinetics as a function of temperature and pH were reported. The loading and encapsulation of Cytochrome C, along with some more interactions with bio-molecules, are discussed in the next section.

## 1.4 Interaction with bio-molecules

NPs can interact with a number of biomolecules, some of these include DNA, SiRNA, proteins like biotin, peptides, enzymes and antibodies. Biomolecules improve the specificity and molecular recognition of NPs. [52] The interactions between inorganic NPs and biomolecules are similar to the ligand modification or chemical modification of NP surface. The common techniques used for such interactions are

- Binding with ligand.
- Electrostatic attraction.
- Covalent binding.
- Conjugating with target specific receptors.

Polymeric NPs can also take up biomolecules like proteins or drug.[53] This is done by absorbing the biomolecule on the NPs. This process of binding or

absorbing is called loading or encapsulation. The purpose of encapsulation of certain molecules is to

- Shield it from the surrounding environment.
- Stay active for longer period (in case of drug).
- Reduce its impact to the surrounding (if it is toxic).
- Release the molecule only in response to stimuli.
- Control the release of the molecule.

DNA is widely used for binding with NPs as they can store genetic information and can also collect information from its surroundings.[54, 55] The detectability of NPs bound with DNA is extremely high even at low concentrations.[56] DNA can be attached to an NP by ligand modification method and usually a large quantity of DNA is added with NPs and the unbound DNA can be removed by methods like centrifuging. DNA can interact with groups like -OH, -NH2, -COOH, -SH.[57]

DNA can be easily attached to Au surface by a gold-thiol bond.[58] Often single stranded DNA is used for interactions with NPs as it is flexible and can be in coiled form.[59] It has been suggested that single stranded DNA easily interacts with Au NPs coated with citrate than double stranded DNA due to higher surface charge density. [60] Other factors that play an important role when NPs interact with DNA are the length of DNA, temperature - for longer DNA, size of NPs.

Biomolecules like drugs can be added *post situ*, by adding the NPs to a concentrated solution of the drug. This is called breathing-in mechanism[61] and the drug is usually added to dried polymeric NPs in a solvent preferred by the polymeric NPs. The NPs swell up as they absorb the drug. A successful encapsulation needs a good compatibility between the NPs and the biomolecule. The NPs and the biomolecule should be stable during encapsulation and in case of NPs with co-polymers, the ratio among the co-polymers play an important role in the extent of encapsulation. The amount of biomolecule present in the NPs and relative performance can be assessed by loading efficiency and encapsulation efficiency. These are shown in equations below.

$$\text{Loading efficiency} = \frac{C_0 - C_t}{C_0} * 100 \tag{1.1}$$

$$\text{Encapsulation efficiency} = \frac{C_0 * \text{Loading efficiency}}{100 * C_N} \tag{1.2}$$

where, $C_0$ is the initial concentration of drug, $C_t$ is its concentration after loading and $C_N$ is the concentration of NPs used.

Fe@Au-PNIPAm NPs, discussed in the previous section, were used in a study to observe their loading properties. The drug Cyt-C was used in the process and a comparative loading between the bare polymeric NPs and the hybrid NPs were studied. It was found that there was decrease in the loading efficiency when NPs were incorporated into the polymers. It was hypothesized that the drug binds with empty sites in the polymeric chains and as the Fe@Au NPs occupy these sites in hybrid NPs, a reduction in loading was expected. The release of drug when subjected to changes in temperature and pH, due to reduction in size, was studied. The NPs were able to release the drug over a long period of time and could be used for drug delivery.

## 1.5 Applications of Multifunctional NPs

In the previous sections, the multifunctionalities of various NPs and their synthesis routes were discussed. In this section application of certain NPs in different fields are presented.

### 1.5.1 Theranostics applications

The word theranostic, a portmanteau, is a combination the of words therapeutics and diagnostics. In such applications, the NPs can both diagnose and act as therapeutic agents. One of the important tasks in all of these applications is to make the multifunctional NPs biocompatible and non-toxic so that they are not rejected by the body. This can be achieved by constricting multifunctional NPs with a biopolymer. Zhang *et al.* synthesized a new class of superparamagnetic multifunctional NPs with magnetite, PEG and folic acid.[62]

Magnetite NPs of 10 nm were synthesized from ferric chloride by precipitation and the NPs were functionalized with silane followed by PEG with fluorescein and folic acid with fluorescein. The cellular uptake with mouse and human breast cells were studied. The cultured cells were incubated with the NPs and the uptake of NPs by the cells was studied via fluorescence, confocal microscopy. When the cells with NPs were compared against the control cells, the NPs were internalized by the cells and showed that these NPs can further be modified for diagnosis and

therapy.

### 1.5.2 Environmental applications

Multifunctional NPs can be used as environmental tracers, to purify water, detect presence of heavy metals and so on. Nanosorbent is used as a separation media to purify water. When Cerium oxide on carbon nanotube was used, a high level absorption of Arsenic was seen.[63] Kostal *et al,* showed that biopolymers used along with DNA have the ability to bind with heavy metal.[64] Fe NPs, formed by coprecipitation, were used to encapsulate DNA and the multifunctional NPs were further coated with silica. The synthesized multifunctional NPs were tested as a tracer in oil.[56] The DNA from the multifunctional NPs, which was in oil, was recoverable, showing the tracing ability of the NPs.

### 1.5.3 Catalytic applications

NPs have been widely used as catalysts for a number of reactions, semiconductor NPs are widely used for photocatalytic/voltaic applications. $TiO_2$ and $SiO_2$ NPs are widely studied for such applications. However, when multifunctional NPs like dumbbell shaped or core-shell NPs were used, there was an increased catalytic effect and it was attributed to surface modification, lattice mismatch and electron interaction at the surface. Wang *et al.* developed a robust routine to synthesize noble metal- metal oxide dumbbell NPs for catalytic uses.[65] Initially the noble metal was organically synthesized and the obtained NPs were used as seeds during thermal decomposition of $Fe(CO)_5$ to $Fe_2O_3$. The resulting multifunctional NPs were dumbbell shaped with noble metal at one end and Fe at the other. This technique was used to synthesize a number of multifunctional NPs like Pt-Fe, Au-Fe, Ag-Fe and Pd-Fe. These multifunctional NPs were used as catalyst for oxidation of CO. When a standalone noble NP is used, there is a significant reduction in catalytic activity and this can be prevented when noble metal-metal oxide NPs are used. It was found that these were very active compared to their normal counterparts.

### 1.5.4 Sensor applications

The inherent properties of inorganic NPs make them an ideal candidate for sensing applications, however, in certain cases NPs can be bound with other molecules and these modified NPs can be used for sensing. In a study by Wu *et al.* magnetic NPs

were used to sense dopamine(DA).[66] Magnetic NPs were prepared by co precipitation method and were coated with PEG silane. This was then functionalized with beta cyclodextrin(CD).

An experimental setup was built to check the ability of CD to detect DA by molecular recognition. The setup consisted of an electrochemical detector, electrodes, magnet and a buffer solution containing DA and NPs. It was suggested that DA and CD form a complex and the formed complex is on top of the magnetic NPs, which can be spatially manipulated using a magnet. The as formed complex moved towards an electrode which can detect the presence of DA. Similar molecular recognition based sensors are being used to detect other materials like pollutants, heavy metals and harmful chemical etc. [67, 68, 69]

The aim of this project was to synthesize multifunctional hybrid NPs containing inorganic and polymeric NPs. As discussed earlier in this chapter, synthesizing hybrid NPs leads to loss of certain properties. The motivation behind synthesizing new hybrid NPs was to overcome the above mentioned loss. This thesis has focused in developing new techniques to form hybrid NPs and understand their properties. The procedure used to synthesize and characterize these NPs and analysis of the results obtained are discussed in the following chapters.

Chapter 2

# Material and Methods

The chemicals used to synthesize different inorganic, polymeric and hybrid NPs and the synthesis routes and characterization tools used are discussed in this chapter.

## 2.1 Materials

The following chemicals were used during this study. Hexadecyltrimehtylamonium bromide (CTAB), Ascorbic Acid (AA), Silver Nitrate ($AgNO_3$), Oleic acid (OA), Gold(3) chloride trihydrate ($HAuCl_4$), Sodium citrate (Na-citrate), Sodium dodceyl sulphate (SDS), Potassium persulphate (KPS),
N,N'-Methylenebis(acrylamide) (BIS), N-isopropylacrylamide (NIPAm), Acrylic Acid (AAc), Iron pentacarbonyl, octadecene and oleylamine(O(AM)2).

### 2.1.1 Dynamic Light Scattering (DLS)

Particles suspended in a solution are in a state of Brownian motion. DLS uses Brownian motion and scattering og light to and calculates the sizes of such particles by measuring their diffusion coefficients.

$$d(H) = \frac{k_B T}{3\pi\eta D} \tag{2.1}$$

where, $k_b$ is the Boltzmann's constant, T is absolute temperature, $\eta$ is the viscosity and D is the diffusion coefficient. The diffusion coefficient is used in Stokes-Einstein equation to find the hydrodynamic radius of particles. The particle in suspension will constanlty move due to Brownian motion. This results in fluctuation in the intensity of light scattered by them. These fluctuations are used

to find average diffusion coefficient by an auto-correlator.

DLS also gice information about the size distribution via the polydispersity index(PDI). This is calculated by using the second moment($a_2$) obtained from the auto-correlation function that is used to find the diffusion coefficient and is given by

$$PDI = \frac{2a_2}{a_1^2} \tag{2.2}$$

Malvern Zetasizer ZS©, shown in Fig2.1 was used to measure the sizes and zeta potentiasl of all NPs synthesized for this thesis.

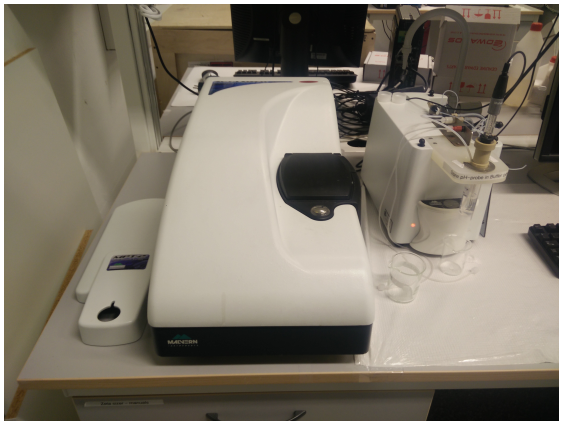

**Figure 2.1:** Malvern Zetasizer Nano-ZS.

### 2.1.2 UV-Vis Spectrometer

UV-Vis spectrometer was used to detect the presence of Au NPs or polymeric NPs by measuring their absorbance values. A solution containing these particles will absorb some of the incident UV-Vis radiation. A detector in the instrument will capture the change in intensities of incident and transmitted rays. Absorbance of such solution is calculated by Beer Lambert's law, which is shown in Eqn2.3

$$log_{10}(I_0/I) = A = \epsilon lc \tag{2.3}$$

Where, $I_0$ is the intensity of incident light, I is the intensity of transmitted light, A is absorbance, $\epsilon$ is the extinction coefficient, l is the path length and c is the concentration of the solution.

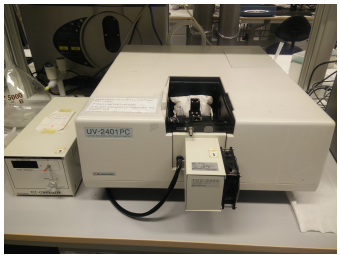


**Figure 2.2:** UV-Vis spectrometer.

### 2.1.3 Scanning Transmission Electron Microscopy (S(T)EM)

The interaction between electrons and the sample on which these electrons are focused is the basis of this type of microscopy. The electron gets scattered after this interaction and several detectors are used to capture and render images of the sample.

Hitachi S-5500, shown in Fig2.3, was used to characterize the NPs synthesized.The samples were analyzed using the Bright field (BF). In this mode, only tranmission electrons interact with the sample and these scatter at relatively lower angle. The samples were observed by dropping them on a Formvar Carbon coated, 300 mesh copper TEM grids and operating the equipment in BF mode.

**Figure 2.3:** Hitachi S-5500 STEM.

## 2.2 Synthesis of Au NPs

Four different shapes of Au NPs were synthesized for this study, namely, spherical NP (Au NSs), nanorods (NR), etched nanorods (ER), nanomakura (NM). Of these shapes, different sizes of Au NS (Au NS 1 -4) were synthesized. Au NS 1 was synthesized by modified turkevich method, Au NS 2-4 were synthesized by a simple citrate method and the anisotropic NPs were synthesized by seed mediated growth. The methods to synthesize these are discussed in the subsequent sub-sections.

### 2.2.1 Spherical Au NPs

Au NS1 was synthesized by a modified Turkevich method using $HAuCl_4$ and Na-citrate.[70] 100 ml of 1mM solution of $HAuCl_4$ was heated with a condenser. The solution was heated until it started to refulx and 10ml of 38.8mM Na-citrate was added and the system was refluxed for another 20 minutes. The solution was allowed to cool to room temperature.

Au NSs2-4 were synthesized by gradually adding 10ml of certain concentrations of $HAuCl_4$ to 10ml of 10mM solution of Na-citrate at 70°C. Different concentrations of $HAuCl_4$ were used to obtain different sizes. Higher concentration of gold solution gives bigger particles. The concentrations used were 0.9mM, 1.5mM and 3.4 mM to get Au NS2 . Au NS3 and Au NS4 respectively. The reaction was stopped after 20 minutes and the reaction mixture was centrifuged for 45 minutes at 1100rpm. The precipitate obtained after centrifuging was redispersed in 10 ml of MQ water.

### 2.2.2 Synthesis of anisotropic Au NPs

In this procedure, a seed solution was added to a growth solution containing reducing agent to obtain desired NPs.[14] The seed solution was prepared by adding 5ml of 0.5mM $HAuCl_4$ to 0.2m $CTAB$. A freshly prepared solution of 3.75mM $NaBH_4$ was added to it after 10 minutes. The mixture was kept stirring for another 2 minutes and the seeds were allowed to grow for 30 minutes.

The growth solution was prepared by adding 1.2gm of $CTAB$ in 15 ml of MQ water with OA if required, details of which are shown in Table2.1. The solution was maintained at 35°C at a constant stirring of 500 rpm. 750 $\mu$l of 4mM $AgNO_3$ was added, followed by addition of 15ml of 1mM $HAuCl_4$ was added. After 15 minutes, the stirring speed was increased to 1000rpm and AA followed by 96$\mu$l of the seed solution were added and stirring was stopped. The overall reaction procedure is shown in Fig2.4.

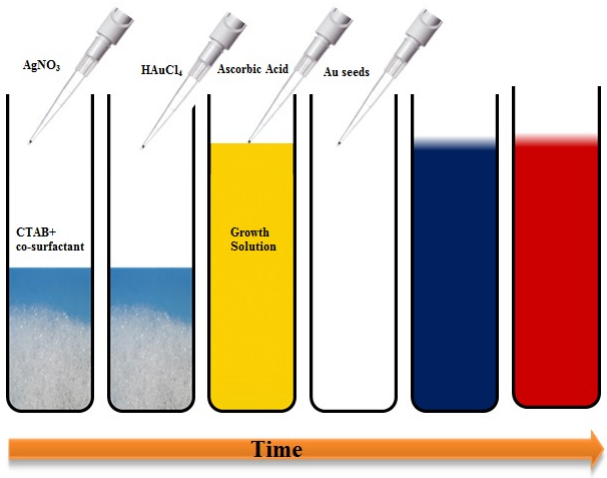


**Figure 2.4:** Schematic representation of the synthesis routine.[14]

The reaction was allowed to run overnight. In case of AuNM, 300$\mu$l of the growth solution was used as seed and added to another growth solution. To summarize, AuER and AuNR were prepared by a single seeded method and AuNM was prepared by double seeded method. The formed NPs were centrifuged at 11000rpm for 40 minutes and re-dispersed in 5 ml of water

| | CTAB | OA | HAuCl4 | AgNO3 | AA | Seed |
|---|---|---|---|---|---|---|
| Nanorods(NR) | 1.2g) | - | 15ml | 700($\mu$l) | 135($\mu$l) | 96 ($\mu$l) |
| Etchedrods(ERs) | 1.2gm | 20($\mu$l) | 15ml | 700($\mu$l) | 135($\mu$l) | 96($\mu$l) |
| Nanomakura(NMs) | 1.2gm | 30($\mu$l) | 15ml | 700($\mu$l) | 135($\mu$l) | 96($\mu$l) |

**Table 2.1:** Chemicals used to synthesize NPs.

## 2.3 Synthesis of Fe@Au

Fe@Au NPs were synthesized by the method reported at Ugelstad Laboratory, as discussed in Section1.3.3. In this technique, Fe NPs were first prepared and then these were coated with Au. Fe NPs were synthesized by thermal decomposition of $Fe(CO)_5$ under inert condition. A mixture of octadecene and O(Am)2 was heated to 120°C for 30 minutes under argon atmosphere. The temperature was increased to 180°C and $Fe(CO)_5$ was injected and the reaction was allowed to proceed for 20 minutes followed by cooling. Fe NPs, thus formed, were separated, washed and dried.

5gm of Fe NPs was dissolved in 10ml 0f 10mM Na-citrate solution and sonicated at 80°C for 30 minutes. This solution was heated to 70°C and 10ml of 1.5mM solution of $HAuCl_4$ was added to it drop by drop. The reaction was stopped after 20 minutes. Fe@Au NPs were centrifuged for 20 minutes at 14000rpm and re-dispersed in 10ml of water.Fig2.5 shows Fe@Au that was synthesized using this procedure.

**Figure 2.5:** Fe@Au NPs

### 2.3.1 Synthesis of Polymeric NPs

The polymeric NPs or nanogels (NGs) were synthesized by modifying the synthesis routine suggested by Sulalit *et al.*.[15] In this procedure, NIPAAm, AAC and BIS were used in a molar ratio of 85:10:5. SDS and KPS were used as surfactant and initiator respectively. In a typical reaction, 180gm of NIPAAm and 14 gm of BIS were added to a round bottom flask, maintained at 70°C. 10 ml of 4.2 mM SDS solution was added to it and kept stirring for one hour. The temperature used was above the LCST temperature and thus the monomers must be in a collapsed state. After one hour, 124 $\mu$l of AAc and 400 $\mu$l of 103mM of KPS were added to the reaction mixture and kept stirring at 250rpm for three more hours. These NGs were dialysed overnight in MQ water to remove unreacted monomers.

Three variations of this reaction were tried as a part of this thesis.

- The entire reaction was carried out under $N_2$ atmosphere with magnetic stirring (continuous method)
- The reaction mixture was stirred with a magnet and nitrogen was used only while adding the initiator (flashing method)

- Nitrogen was used only while adding initiator and the reaction mixture was stirred with an impeller (impeller method)

Fig2.6 shows the impeller setup that was developed and used during this study.

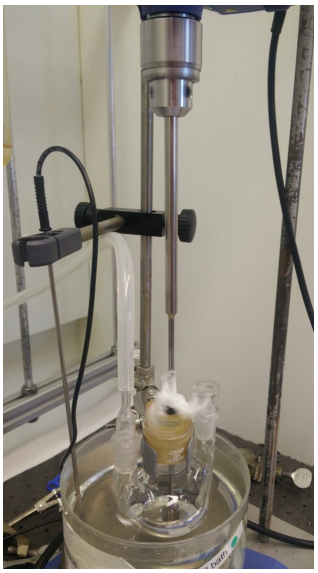

**Figure 2.6:** Impeller method

### 2.3.2 Synthesis of hybrid NPs

For the rest of the report hybrid NPs refer to different combination of polymeric NPs with inorganic NPs. These hybrid NPs were synthesized using a procedure similar to the one discussed in the previous section. Here, different volumes of 3 mg/ml of NP solution were added to reaction mixture of NIPAAm, BIS and 5ml of 5.4mM SDS. The mixture was heated at 70°C for one hour and 54 $\mu$l of AAc and 400 $\mu$l of 210mM KPS were added. The reaction mixture was kept under nitrogen atmosphere when KPS was added. The reaction was allowed to run for 2 hours. Depending on the type of inorganic NPs used, either a magnetic stirrer or an impeller was used. After completion of reaction, the formed hybrid NPs were dialysed overnight.

Fig2.7 is a schematic diagram of the processes that produce NGs or NGs with inorganic NPs.

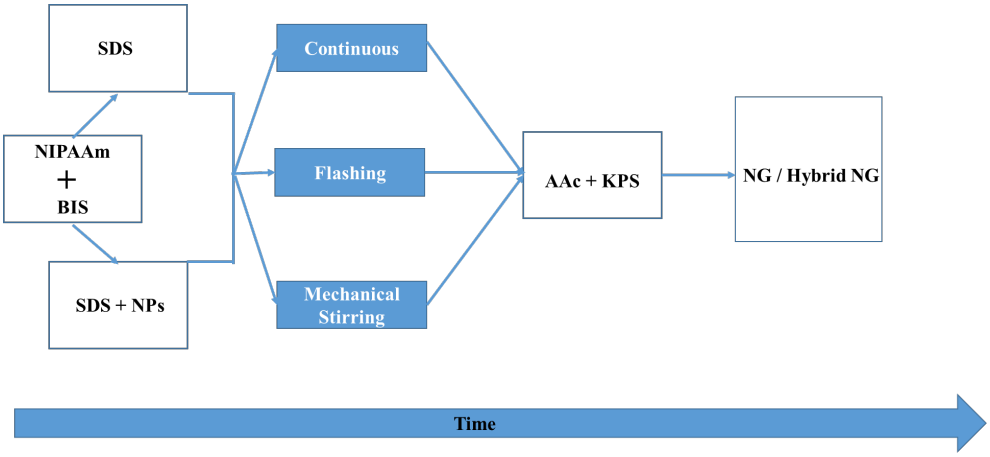


**Figure 2.7:** Schematic diagram showing various routes that were used to synthesize NGs or hybrid NPs

### 2.3.3 Functionalization of Au NPs

Au NPs were functionalized with different ligands to study the effect of these ligands on polymerization reaction. Au NPs were functionalized with PEG or P-lysine. Au NPs were functionalized with PEG by adding 1mg of PEG to a solution of 1mg/ml of NPs. The mixture was shaken for 2 hours. These were then centrifuged at 14000rpm for 20 minutes and redispersed in 1ml of water.

To functionalize with P-lysine, 1 ml of 1mg/ml of NPs was mixed with 200$\mu$l of 0.01 mg/ml of P-lysine for 2 hours. After this, 200$\mu$l of P-lysine was added and shaken for 2 more hours. The reaction mixture was then centrifuged at 14000rpm for 20 minutes and redispersed in 1 ml of water.

### 2.3.4 Dialysis

Unreacted monomers and unused SDS in NGs and hybrid NPs can be effectively removed by dialysis. The dialysis tube used for this process was washed with MQ-water and the samples that needed dialysis were pipetted into dialysis tube and clamped. This tube was placed in a beaker with MQ-water with slow stirring at 100rpm for 24 hours.

## 2.4 Time based study

Growth of NGs was studied by drawing samples at different time points during the reaction. A predetermined volume of the growing NGs was dropped into ice-cold water. Depending on the study, the lost sample was either replenished with same volume of water at 70°C or not replenished at all. These samples were then analyzed using DLS.

## 2.5 VPTT calculation

The VPTT of NGs obtained from the three methods, along with hybrid NGs were calculated by plotting the swelling and collapse of these NPs over a temperature range, both while heating and cooling.[14] The sizes of these NPs were measured between 25° and 55°C at a step interval of 5°C. From these data, a parameter $\alpha$ was calculated. $\alpha$ represents the swelling of these NPs and is described in Eqn 2.4

$$\alpha = \left\{ \frac{D}{D_0} \right\}^3 \tag{2.4}$$

where D is the diameter at a given temperature and $D_0$ is the diameter at room temperature. The parameter $\alpha$ was plotted against temperature for heating and cooling cycles and a sigmoidal 5 parameter equation was fitted to the curves obtained.A point in the middle of the the curve was chosen and the area under the curve on either side of the point was calculated and the point is adjusted and the process is repeated until both areas become equal. The corresponding temperature is the VPTT of the system. The MATLAB code used for this model was developed by Sulalit*et al.*[14]

Chapter 3

# Results and Discussion

A summary of results obtained from various experiments done and the details inferred from these are presented in this section. The first part of this section consists of results obtained from characterizing the inorganic NPs used. This is followed by characterizing polymeric NPs (NGs)and a comparative analysis of different method used to synthesize these NPs. The results obtained from time based study of these methods are discussed. The final part consists the analysis of hybrid NPs. Hybrid NPs refer to inorganic NPs in NGs. This part outlines the result of different combinations of NPs and NGs that were tried. Finally, an analysis of the hybrid NPs based on the properties of its constituent inorganic NPs are presented.

## 3.1 Inorganic NPs

Au NPs of different sizes, shapes and Fe@Au NPs were synthesized using the procedure discussed in sections 2.2,2.3. The NPs obtained from these reactions were characterized using DLS, UV-Vis and S(T)EM. The results from these techniques were compared against existing literature.[49, 14]

The results from UV-Vis and S(T)EM are shown in Fig3.1.

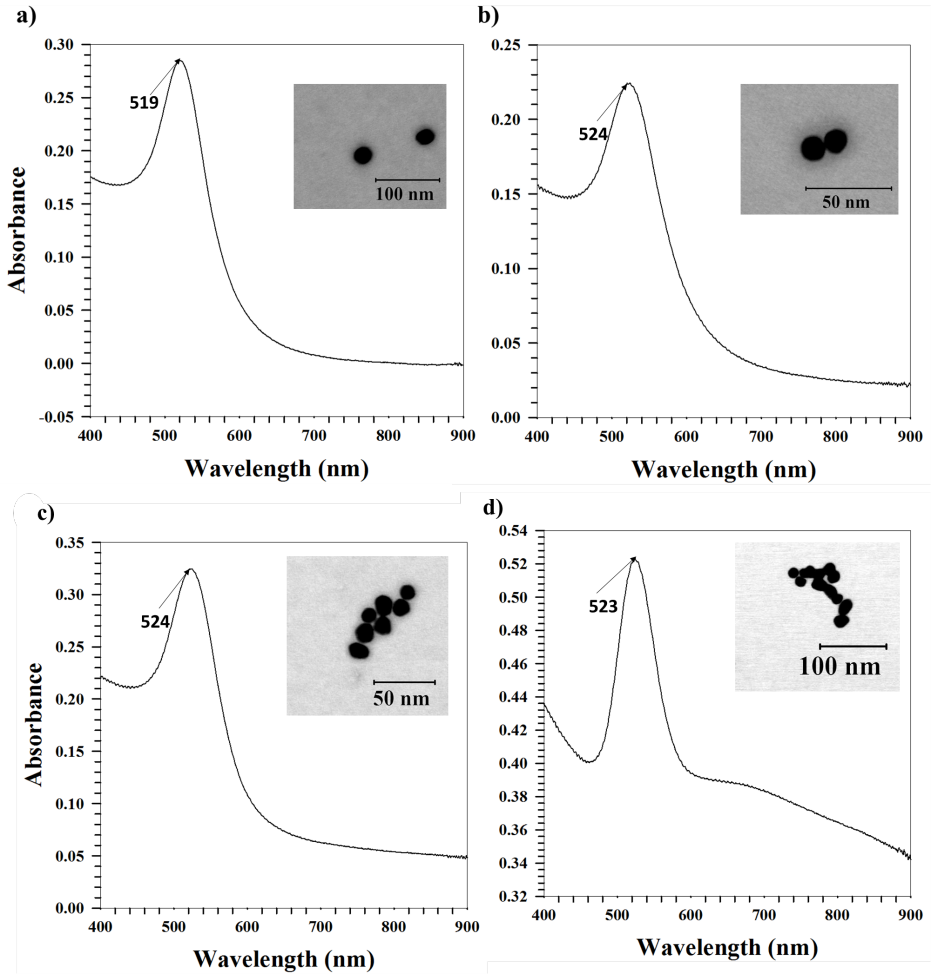


**Figure 3.1:** UV-Vis spectra showing LSPR peak and corresponding S(T)EM images of a) Au NS 1 b) Au NS 2 c) Au NS 3 d) Au NS 4

Fig3.1 shows UV-Vis data obtained for Au NSs 1-4. As these are spherical in shape, only one peak is observed for each of these NPs. This peak represents Localised Surface Plasmon Resonance (LSPR) peak[1]. The actual LSPR peaks are marked on the respective graphs.

Anisotropic NPs were synthesized by a seed mediated procedure. This method gives uniform NPs. Fig 3.2a),b) shows the UV-Vis spectra obtained for NR and ER

[1]When an incident radiation matches the energy if electrons on surface, a resonance is achieved and can be seen as a peak in UV-Vis

respectively. The multiple peaks seen in these graphs correspond to multiple axes of these NPs.The two peaks observed correspond to the transverse and longitudinal axes respectively. In case of ER, an additional peak is observed at 600nm. This is due to the etching in the centre of ER morphology, as seen in its corresponding S(T)EM image. This correspondsto etching reported in literature. It has been suggested that this etching could be due to presence of OA.[14]

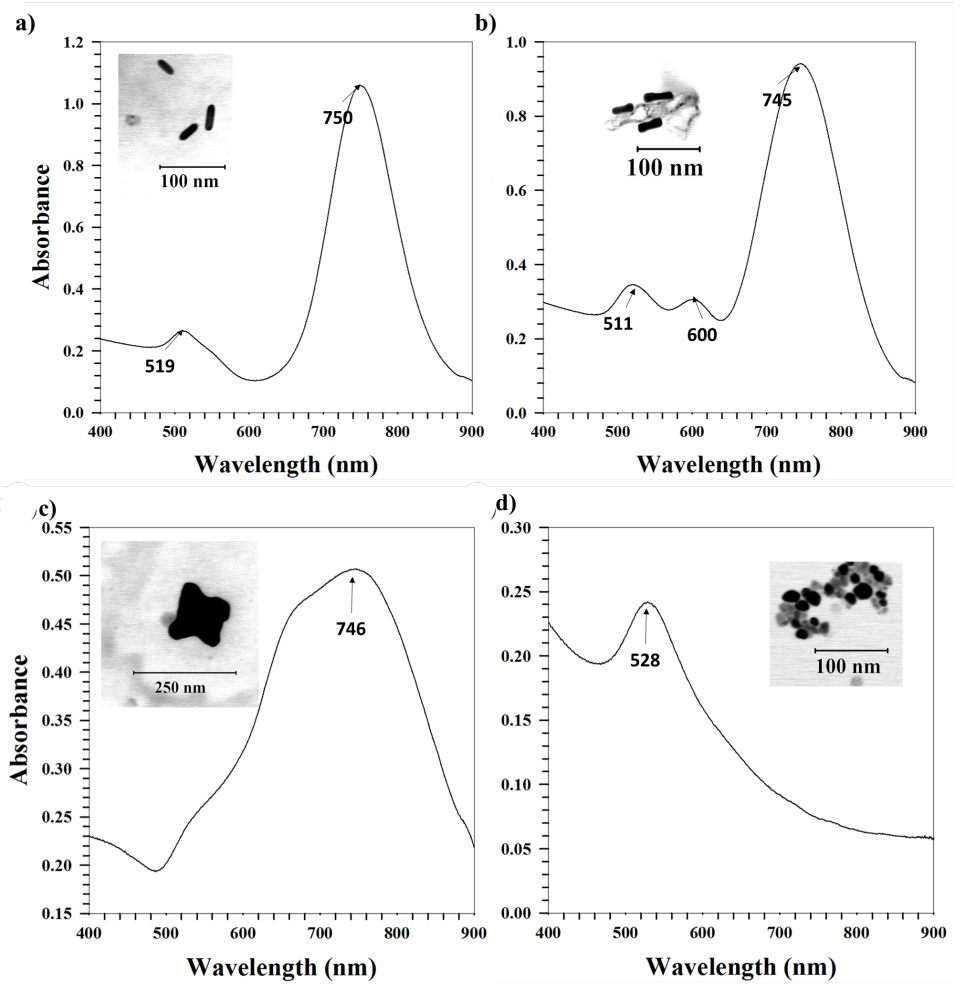


**Figure 3.2:** UV-Vis spectra showing LSPR peak and corresponding S(T)EM images of a) NR b) ER 2 c) NM 3 d) Fe@Au

Fig3.2c),d) depicts the LSPR peaks obtained for NM and Fe@Au. NM has multiple faces and axes, hence there is one broad peak rather than having distinctive peaks corresponding to individual axes.[14] The pillow like shape of NM,

with multiple etching, is suggested to be an effect of OA in reaction mixture. Fe@Au NPs are predominantly spherical, however, from the images obtained from S(T)EM, the exact coating of Au over Fe cannot be identified.

The sizes and zeta potentials of these NPs were measured using DLS and the results are shown in the Fig.3.3. All the standard deviations used in the report were calculated from DLC triplicate measurements unless mentioned otherwise.

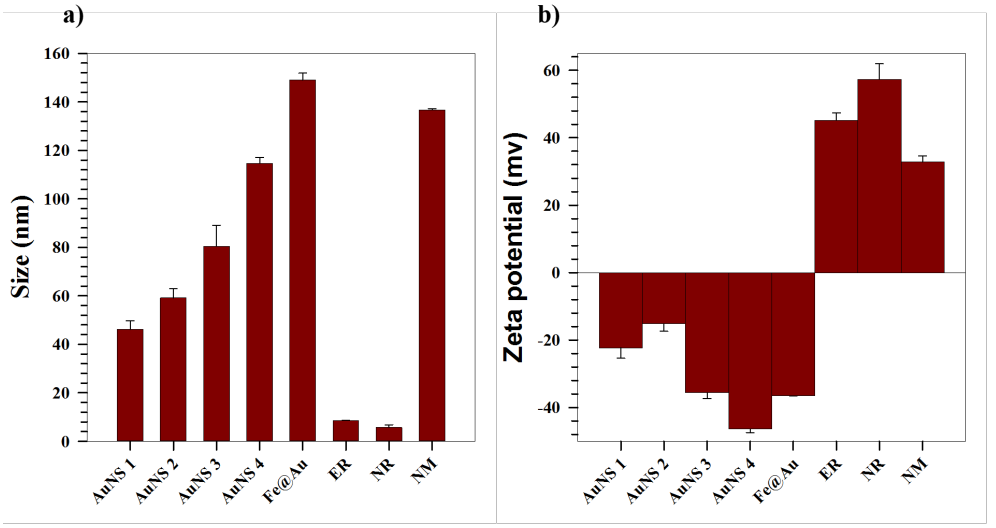


**Figure 3.3:** Sizes and zeta potentials of NPs

From Fig3.3, AuNS 1 is the smallest of all the spherical NPs with a size of 46±4nm while the largest ones are Fe@Au NPs with a size of 150±3nm . As the concentration of gold precursor in reaction procedure increases, there is an increase in the size of NSs. The bigger size of Fe@Au can be attributed to the coating of Au over Fe and a higher concentration (1.5mM) of $HAuCl_4$. As all these NPs are citrate coated, a negative zeta potential is expected in all the cases.

Although the S(T)EM images of anisotropic Au NPs show bigger sizes, the results from DLS in Fig3.3 show that these are small in size. This discrepancy arises as DLS works on the assumption that all particles are spherical in shape. DLS measures hydrodynamic radius and this can also cause some mismatch between DLS measurements and observed sizes from S(T)EM. The zeta potentials of these anisotropic NPs are positive as they have CTAB as capping agent.

### 3.1.1 Characterization of functionalized NPs

Au NS 1 and Au NS 4 were functionalized with PEG and P-Lysine, as described in section 2.3.3. These NPs were then characterized with DLS.

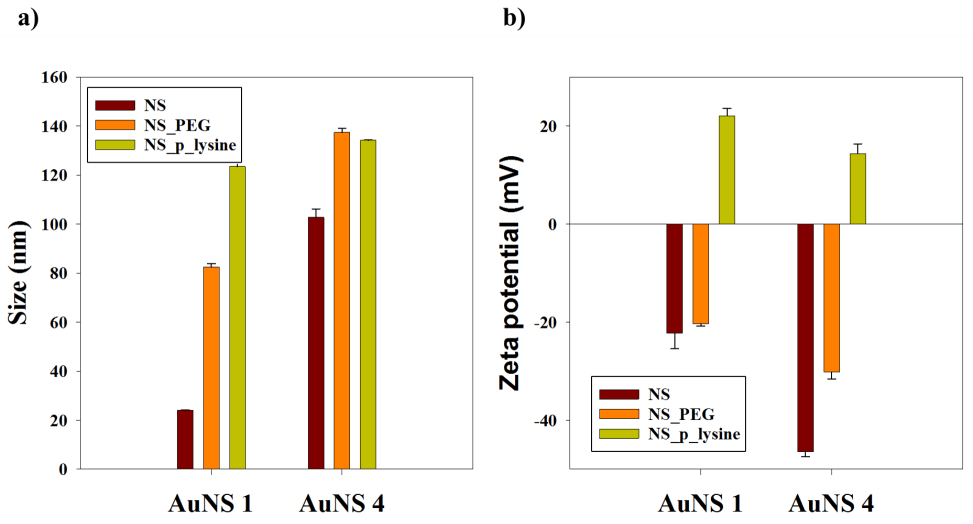


**Figure 3.4:** Sizes and zeta potentials of functionalized NPs

An increase in size can be seen in Fig3.4 and this is due to addition of these ligands. As P-Lysine is cationic, a shift in zeta potential is observed. Increase in sizes along with drastic changes in zeta potentials are good indicators of functionalization. However, in order to reaffirm binding of PEG on to the surface, these NPs were also characterized using UV-Vis as addition of PEG leads to shift in LSPR peak.[49] The red shifts of the LSPR peaks upon coating are shown in Table3.1. The corresponding UV-Vis data are attached in AppendixA

| Au NanoSphere | Peak (nm) | After PEG coating (nm) |
|---|---|---|
| 1 | 521 | 523.5 |
| 4 | 525.5 | 529.5 |

**Table 3.1:** Peak shift of AuNSs after PEG coating

## 3.2 Synthesis and characterization of Nanogel

NGs were synthesized by the procedure given in section2.3.1. This procedure was repeated several times to check its reproducibilty. Similar NGs were obtained during these repeats.An example of such NGs(NG1 and NG2), that were synthesized at different times, their sizes and volumteric collapse efficiencies (VCEs) are shown in Fig3.5. VCE is the percentage decrease in volume of NGs after collapse and can be calculated by

$$\text{VCE} = \frac{\text{Volume at } 25°\text{C} - \text{Volume at } 45°\text{C}}{\text{Volume at } 25°\text{C}} \tag{3.1}$$

The sizes of these NGs were 218±2 and 208 ±2 with a VCE of 92 and 91 respectively. The standard deviation is calculated from three measurements of the sample. These NGs collapse at 45°C and the solution turns turbid at this temperature.

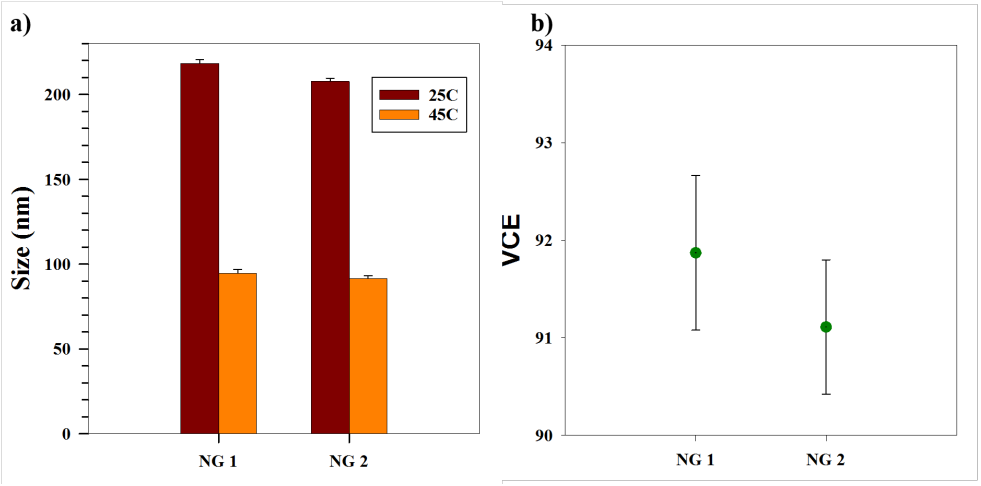


**Figure 3.5:** a) Sizes at different temperature of NGs b) VCE of NGs.

These NGs were found to be stable having zeta potential around -15mV. When these NGs collapse, the zeta potential increases further. These are shown in Fig3.6. The zeta potentials of all the NGs and hybrid NGs synthesized during this thesis were high and hence it was concluded that stability is not an issue with these NGS. Therefore, sizes and collapse of these NGs and hybrid NPs will only be discussed throughout the report.

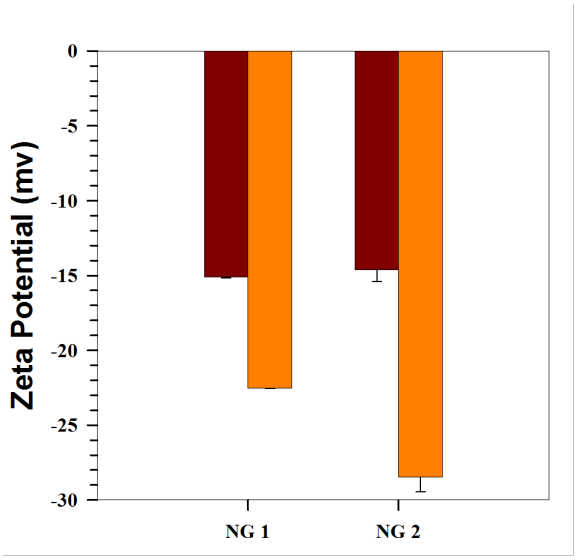


**Figure 3.6:** Zeta potentials at different temperatures of NG1 and NG2 respectively

When the concentration of SDS was changed, the sizes of NGs changed as well. There was a decrease in size of NGs as the SDS concentration increased. When the SDS concentration used was decreased from 4.2mM to 2.1mM, there was an increase in size from 161±1 nm to 257±8. These were recorded before dialysis (BD) and are shown in Fig3.7.

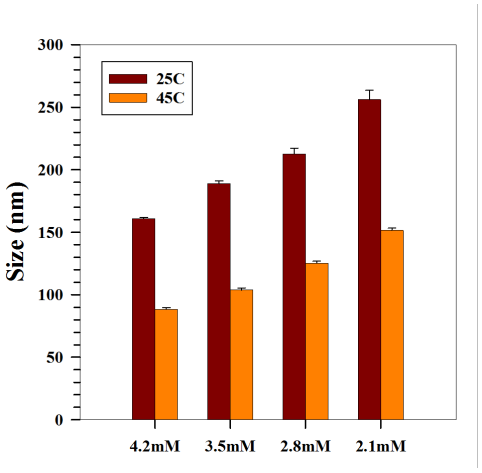


**Figure 3.7:** Sizes of NGs prepared with different SDS concentration

This observation could be due to an increase in stability due to presence of ad-

ditional hydrophobic tails (from SDS). [15] Similar trend can also been seen after dialysis (AD). Another characteristic behaviour of NGs is increase in its size post dialysis. This increase is due to removal of unreacted monomers and unused SDS. However, despite an increase in size, these NGs still collapsed at 45°C. Fig3.8 is a representation of these properties.

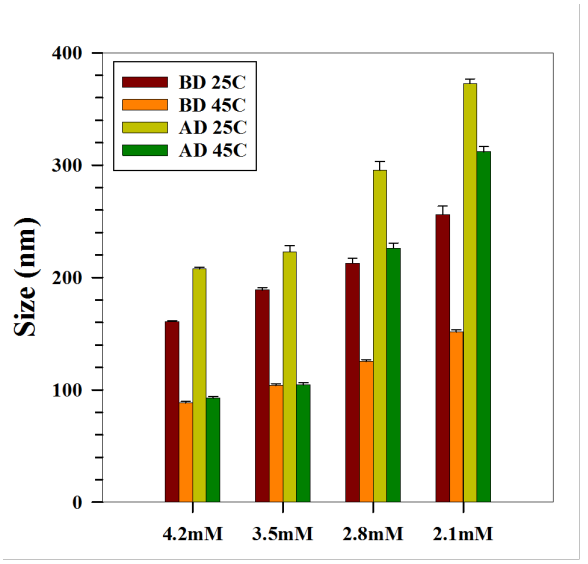


**Figure 3.8:** Sizes of NGs prepared with different SDS concentrations before and after dialysis

Fig3.8 shows the sizes of NGs, before and after dialysis, and their collapses at 45°C. However, there was an observable decrease in collapse of NGs as the concentration of SDS decreases. This can be easily seen in a plot of VCE vs concentration of SDS, shown in Fig 3.9

In this study, VCE decreased from 91% to 41% at 4.2mM and 2.1mM of SDS respectively. In a similar study, it was reported that VCE decreased from 97% at 5.5 mM of SDS to 46% at 2 mM of SDS.[15]

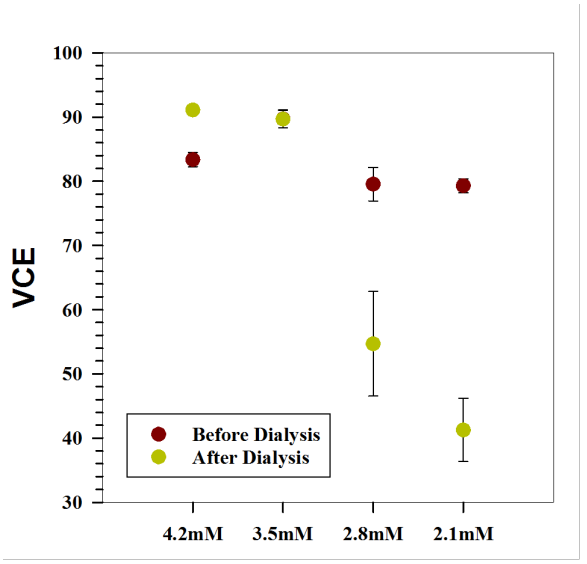


**Figure 3.9:** Volumetric Collapse Efficiencies of NGs

Fig3.10 shows an image taken of NGs synthesized with 4.2mM SDS. The pale spots in the picture, few of which are encirlced, are the NGs. The monodispersity in the system can be seen in the picture.

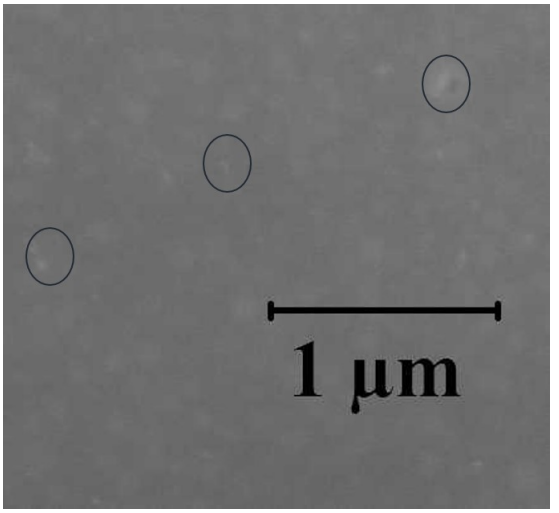


**Figure 3.10:** S(T)EM image of NGs

One of these NGs, NG synthesized with 4.2mM of SDS, was chosen and its dependence on temperature was found by measuring its size at different tempera-

tures. By using the procedure in Section2.5, heating and cooling cycles of this NG were plotted in Fig.3.11

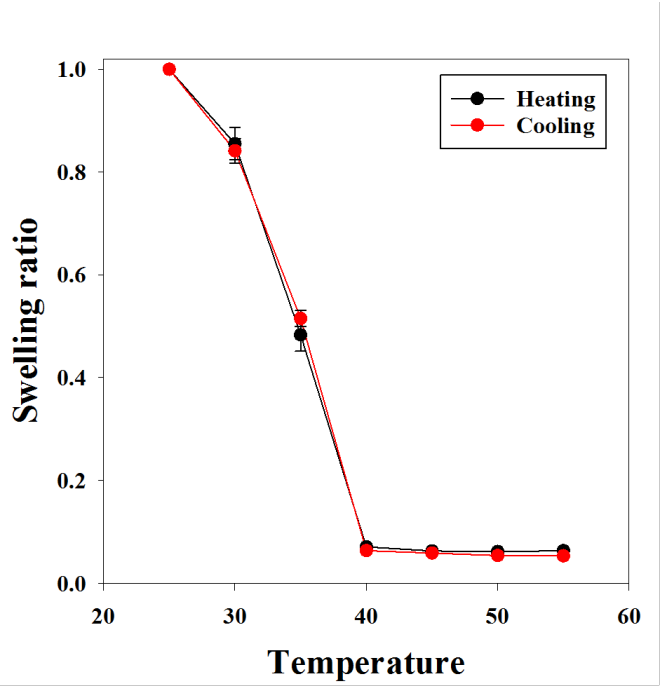


**Figure 3.11:** Temperature dependence of NGs size

Sigmoindal 5 parameter fit was used and the VPTT was found using the method described earlier. The VPTT of this NP was found to be 36.4°C. A sample calculaion is shown in Appendix B. From the trends observed in Figures3.7 to 3.11, S(T)EM and the calculated VPTT, it can be inferred that the polymers obtained are NGs and they have stimuli-responsive properties.

## 3.3 Need for new methods to synthesize NGs

Although NGs can be used for drug release owing to their stimuli response, their functionalities can be increased by using them with other types of NPs. One such hybrid NP was discussed in Section1.3.3, where PNIPAm/AAc/Fe@Au NPs were synthesized. One of the main drawbacks while using magnetic NPs in such processes is loss of NPs due to attractive forces by magnetic stirrer. This can be visually observed, as shown in Fig3.12.

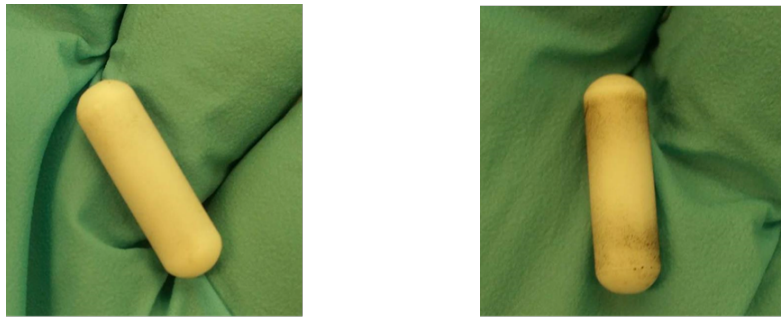


**Figure 3.12:** Magnetic stirrer before and after polymerization reaction

This loss in NPs can directly impact the magnetic properties expected from such hybrid NPs. In order to overcome this problem, a impeller can be used. However, completely sealing such apparatus, for continuous flow of nitrogen, can be difficult due to incorporation of moving parts in the experimental setup. Although a continuous flow of nitrogen was suggested, of all the chemicals used, the initiator KPS is the one that needs minimal contact with air. Therefore, nitrogen could be used only while adding KPS for the setup involving impeller. However, the resulting NGs would be difficult to compare with NGs obtained from regular method as there are two new variables in the setup, change of stirrer and nitrogen flow. Hence an intermediate setup was proposed, this setup will use magnetic stirrer however, nitrogen will be used only while adding KPS. As KPS is an initiator, it was assumed that all of KPS will be used within few minutes after its addition. Therefore, nitrogen was flashed for a time period of 5 minutes after adding KPS. This procedure was followed for flashing and impeller methods.

## 3.4 Continuous, Flashing and Impeller methods

The NGs synthesized from continuous, flashing and impeller methods will be referred as NG_C, NG_F and NG_I respectively. Hydrodynamic sizes obtained from these methods are shown in Fig3.13. NG_F and NG_I increase in size after dialysis. These NGs also collapse at 45°C like NG_C. The characteristic colour change was also observed for these NGs.

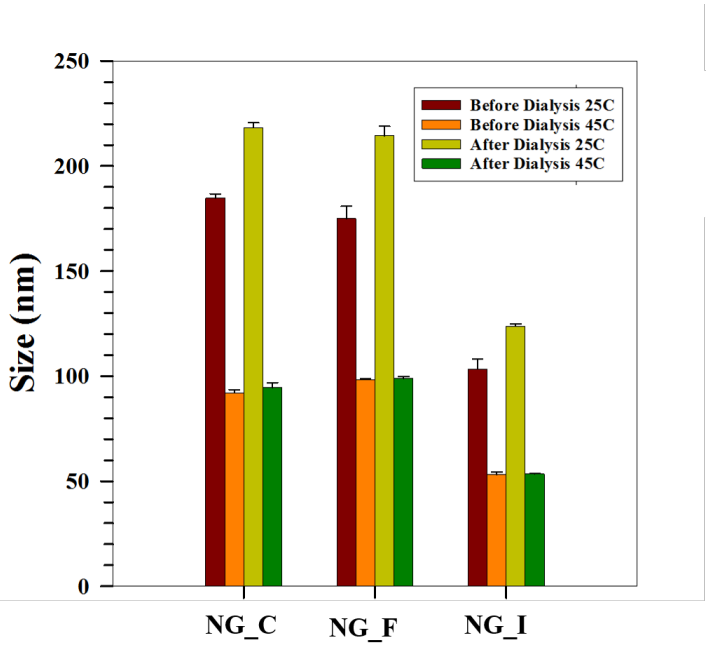


**Figure 3.13:** Size of nanogels before and after dialysis.

A substantial decrease in size of NG_I can be seen in the graph. Despite the smaller size, NG_I has a high volumetric collapse efficiency of 92%. The smaller size obtained could be due to the presence of impeller which can cause a better mixing of solution. This could directly lead to more number of nuclei being formed, there by decreasing the available monomer units for growth of NGs. A similar observation was reported when an impeller was used for crystallization.[71] An alternative explanation for lower sizes could be due to loss of water in the experimental setup for impeller method. High temperature of the reaction and inability to completely seal the experimental set up could lead to loss of water. This continuous loss of water might alter the local SDS concentration and indirectly affect the size as it has been shown that SDS concentration is the most important parameter that controls the sizes of the NGs.[15]

The size dependence of NGs on SDS concentration was checked for these methods and are shown in Fig3.14.

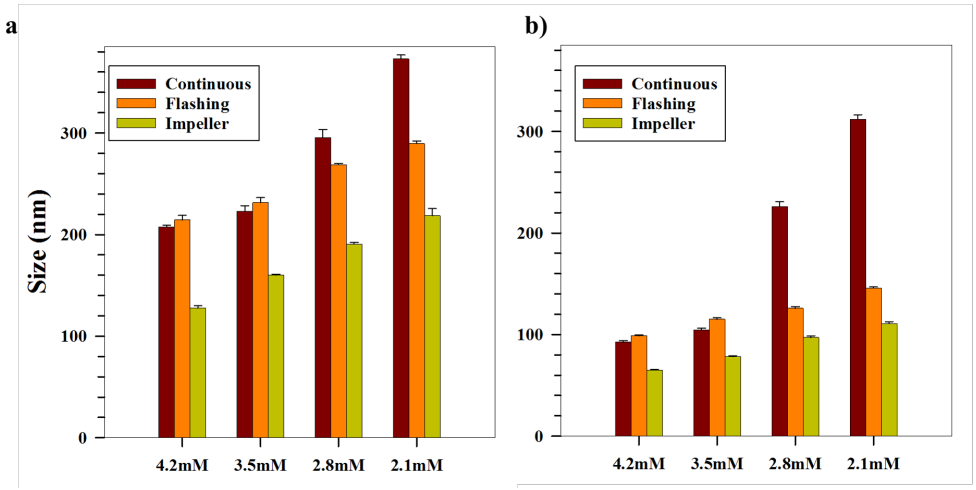


**Figure 3.14:** Sizes of NGs synthesized by continuous, flashing and impeller methods at a)25°C b)45 °C

Fig3.14 depicts the increase in sizes of NG_F and NG_I as SDS concentration decrease. Sizes of NG_I were smaller than others at each concentration of SDS. Unlike NG_C, at 45°C, the collapse of NG_F and NG_I is similar at all concentrations of SDS.

Fig3.15 shows the VCEs of these NGs as a function of SDS concentration. NG_F and NG_I has VCEsaround 90% at all concentrations. Although NGs of different sizes can be produced by continuous methods, these NGs do not collapse to same extent. This could be due to the bigger size of these NGs which were around 400nm.

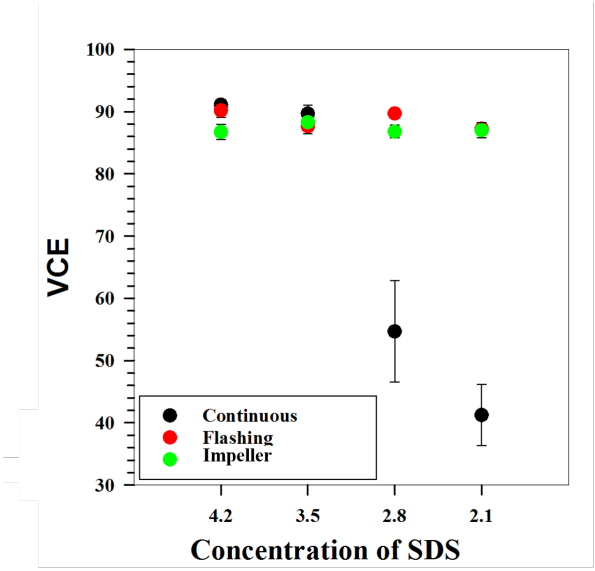


**Figure 3.15:** VCE of NGs synthesized by continuous, flashing and impeller methods.

In such NGs, more pH responsive AAc might be present; a combined change in temperature and pH might increase the VCEs of NG_C when synthesized at lower SDS concentration. In order to understand the growth, timed based experiments were performed for these NGs.

## 3.5 Time Based Studies

The procedure for time based study is mentioned in Section2.4. The impact of solvent loss, as discussed in previous section, was checked by comparing the growth and sizes of two NG_F samples(F1 and F2). Samples were drawn at same time points for both F1 and F2. However, the lost volume was replenished with hot water for F2 and water wasnot added for F1. The sizes obtained at different time points of F1 and F2 are shown in Fig.3.16

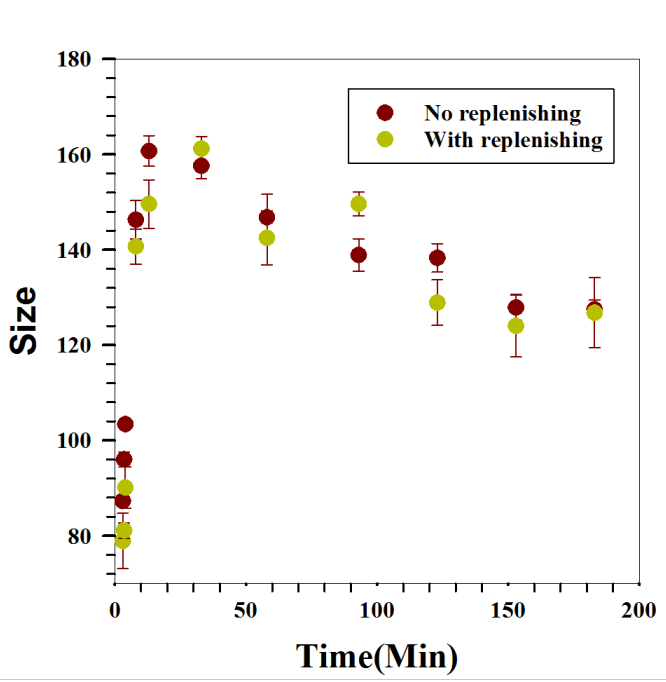


**Figure 3.16:** Size vs Time of samples obtained from experiment without replenishing (F1) and with replenishing (F2).

The final sizes obtained before and after dialysis were comparable and are shown in Table3.2

| | Before Dialysis(nm) | After Dialysis (nm) |
|---|---|---|
| F1 | 128(±) 2 | 170 (±)1 |
| F2 | 127 (±) 7 | 175 (±).2 |

**Table 3.2:** Sizes of samples obtained from experiment without replenishing (F1) and with replenishing (F2).

From the sizes obtained, it can be inferred that loss of solvent does not influence growth of NGs. However, other timed experiments for the three methods were performed by adding solvent after drawing samples.

Once the initiator is added to the reaction mixture, a visible colour change can be seen. The reaction mixture turns to pale white from being colourless. This becomes more whiter as the reaction proceeds.The initial colour change occurs at different time points for the three methods. The colour change was quickest for impeller (around 1-2 minutes) and slowest for continuous (around 10-20 minutes). The colour change for flashing was around 3 minutes. The change is colour is due to the collapse and precipitation of polymers to form the nuclei.

Samples were drawn before the colour change until the end of reaction (3 hours). However, the data from samples before colour change were not considered as the sizes were too big or standard deviations and sizes were of similar orders, as shown in Appendix C. It is assumed that before colour change. the monomers, cross-linker and other chemicals are in the process of reacting with one another and collapsing as well. Hence, the time points before colour change are not used in this section. The time zero in the following plots correspond to the time at which visible colour change is noted. Two experiments were performed for each method and samples were collected at different time points. This was done on assumption that NGs synthesized from same method grow similarly. This helped in collecting more data points to do a preliminary analyses to understand these NGs. Plots of sizes, poly dispersity indices (PDI)[2], VCEs and Normalized sizes against time. Normalized sizes can be found by the Equation3.2,

$$\text{Normalized size} = \frac{\text{Size at given time point}}{\text{Final size}} \tag{3.2}$$

### 3.5.1 Size vs time

The sizes of NG_C,NG_F and NG_I were measured at 25°C and 45°C and plotted against time. The sizes at both the temperature follow a similar trend. All the samples were kept at 45°C for 5 minutes for the polymer to collapse and then the sizes were measured. The plots between sizes and time can be seen in Fig3.17.

[2]Indicates the extent of monodispersity of a sample on a scale of 0-1 with 0 being completely monodispersed. Calculated from second moment of auto corelation function used in DLS

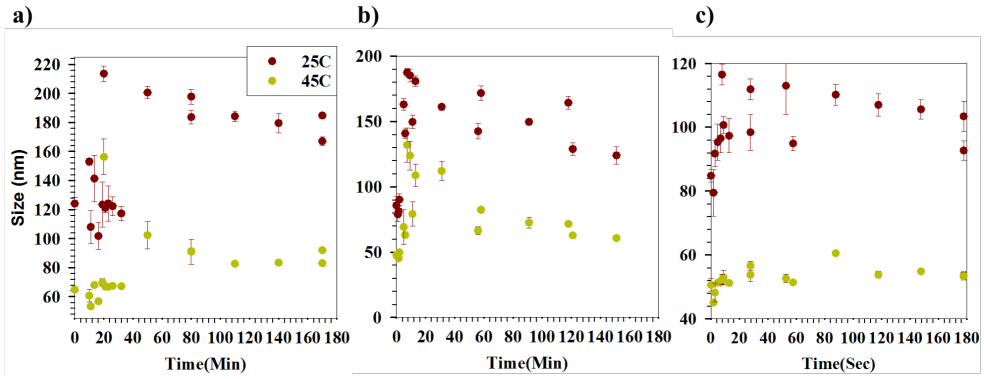


**Figure 3.17:** Size vs Time of NGs synthesized by a) Continuous, b) Flashing and C) Impeller methods.

After the colour change, there is a rapid increase in the size and the size tends to stabilize around 60 minutes. The initial rise in size differs for the three methods. The rise is quickest for the impeller method, occurring within first few minutes. In case of continuous, this rise is most gradual when compared with others. The sizes at 45°C also follow similar trend. The collapse at 45°C can be better visualized with a plot of VCEs as there will be an observable decrease in collapse.

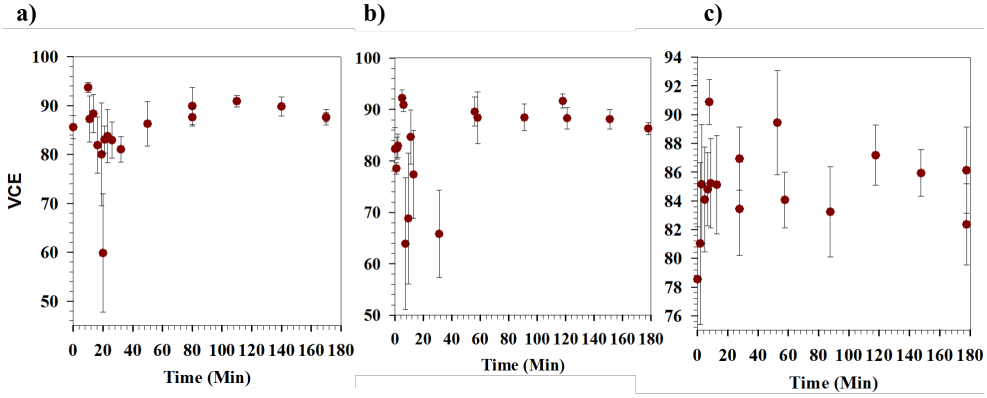


**Figure 3.18:** VCE vs Time of NGs synthesized by a) Continuous, b) Flashing and C) Impeller methods.

Fig3.18 shows that VCEs vary a lot during the initial phase of the reaction. VCE is lowest around 30 minutes for continuous method. Similar trend is seen between 10- 15 minutes for flashing method. In case of impeller, the collapse is almost same but its standard deviation is high around 15 minutes.

All these variations stabilize around 60 minutes for continuous and flashing. VCE stabilizes earliest for impeller. These graphs can be split into two, for early time period and latter time period. For rest of this section, when a graph is split, the time axis will be split as 0-30 minutes and 30-180minutes for continuous and 0-15minutes and 15-180 minutes for both flashing and impeller methods.

During the initial phase of the reaction, as shown in Fig3.19, either VCE is decreasing or standard deviation is high. This could suggest that not all NGs grow uniformly as an uniform growth would result in uniform sizes after collapse and similar VCE values through out the reaction.

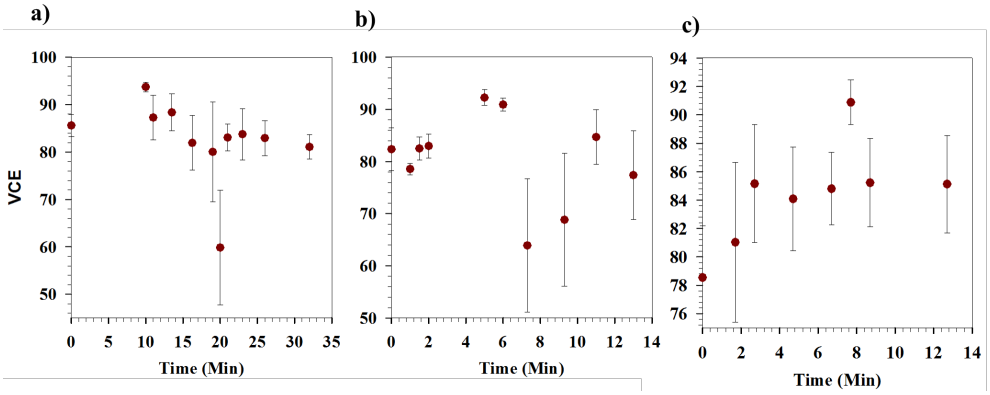


**Figure 3.19:** VCE vs Time of NGs synthesized by a) Continuous, b) Flashing and C) Impeller methods.

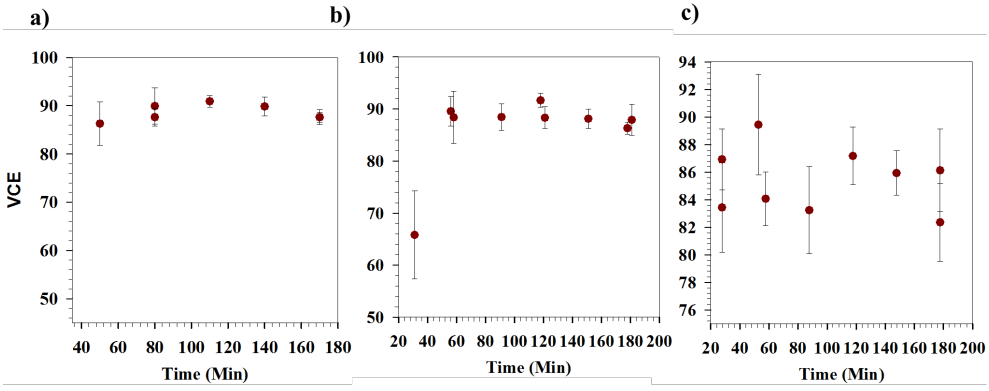


**Figure 3.20:** VCE vs Time of NGs synthesized by a) Continuous, b) Flashing and C) Impeller methods.

Fig3.20 shows a fairly uniform collapse from 90 minutes. There is also a

significant reduction is standard deviation. Growth can also be tracked with PDIs of growing NGs as a function of time. The PDIs of NGs over entire reaction period are shown in Fig3.21

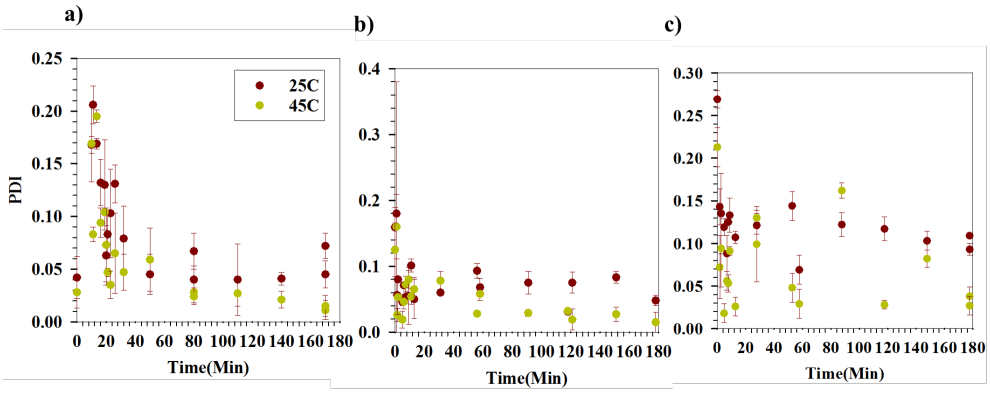


**Figure 3.21:** PDI vs Time of NGs synthesized by a) Continuous, b) Flashing and C) Impeller methods.

Similar to the size plots, PDIs at 25°C and 45°C follow similar trend. In all three plots, there are few time points where the PDI at 45°C is higher than at 25°C. The PDI should be low at higher temperature for these NGs as they collapse at this temperature.[15] The extent of difference in the sizes (or volume) will diminish as the size is reduced. These suggest that not all the NGs collapse as some NGs are newly formed and are too small to collapse or NGs are of different sizes and they collapse to different sizes.

To understand the size distributions of NGs, the PDIs at 25°C are analyzed by splitting the time axis. From Fig3.22, PDI is high for all the methods, suggesting that during the initial phase NGs grow non-uniformly. Similar inference was suggested while comparing sizes and collapse. In case of NG_I, the standard deviation is quite low even from the start of the reactions. It can be interpreted that these NPs grow fairly uniform when compared with NG_C and NF_F.

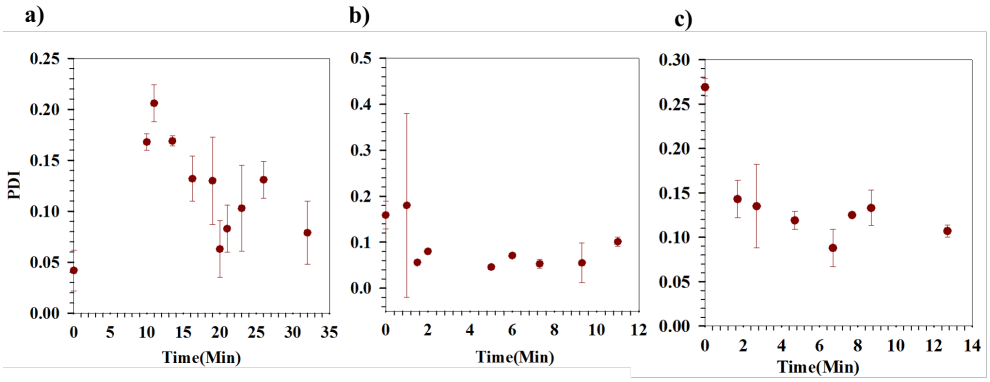


**Figure 3.22:** PDI vs Time of NGs synthesized by a) Continuous, b) Flashing and C) Impeller methods.

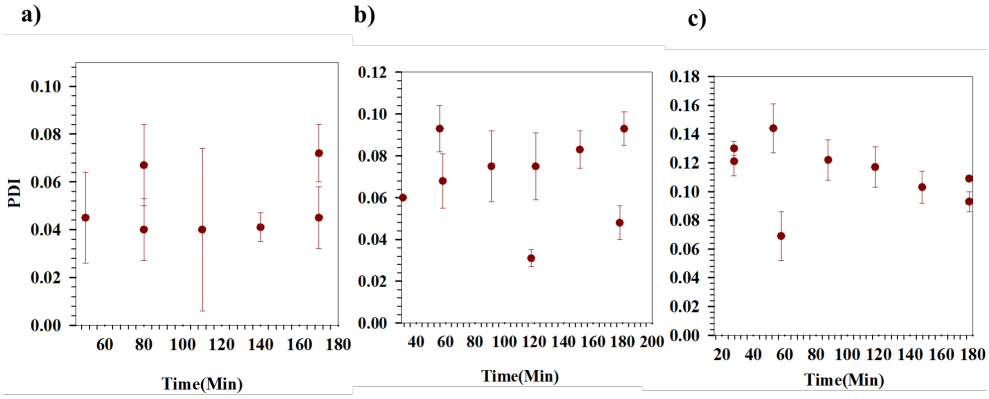


**Figure 3.23:** PDI vs Time of NGs synthesized by a) Continuous, b) Flashing and C) Impeller methods.

Fig3.23 shows the PDIs after the initial phase. NG_C has lowest of PDI among all the NGs, despite having a very large PDI in the beginning. On the other hand, there is not a big difference in PDI of NG_I. VPTTs of these NGs were calculated to further understand them. The effects of method of choice on VPTT of obtained NGs were analyzed by carrying out size vs time plots. The procedure used was similar to the one discussed earlier in Section2.5. The heating and cooling cycles of these NGs are shown in Fig3.24

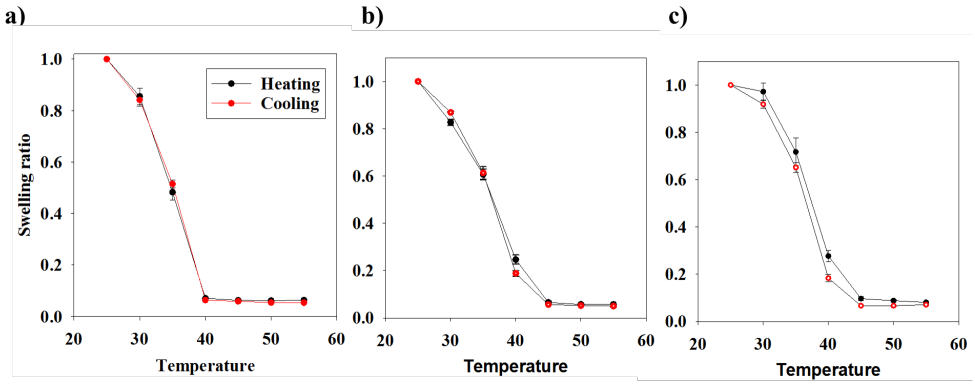


**Figure 3.24:** VPTT of NGs synthesized by a) Continuous, b) Flashing and C) Impeller methods.

All the curves follow a sigmoidal path, however the collapse of NG_C is much steeper than the rest. NG_C, as discussed in earlier subsection, are more monodisperse than the rest. The steeper shift could be because of this as all NG_C collapse uniformly. This will correspond to lower VPTT of NG_C. The VPTT of these NGs are shown in Table3.3

| | VPTT (°C) |
|---|---|
| NG_Continuous | 36.35 ± .05 |
| NG_Flashing | 37.76 ± .1 |
| NG_Impeller | 37.74 ± .06 |

**Table 3.3:** VPTT of NGs synthesized by a) Continuous, b) Flashing and C) Impeller methods

The VPTT of NG_C is lower than the other NGs as these are more monodispersed. These variations in VPTT also makes these NGs to be used at different temperatures.

In order to understand the overall growth of these NGs, the sizes were normalized and plotted against time. The previous plots of size, PDI and VCE helped in understanding the behaviour at each time point of one system. Normalizing the size would help in looking at the overall trends that these NGs follow. It also helps in comparing the trends of different NGs as their relative size differences will not impact the comparison . Such plots can help in developing growth curves to understand kinetics. These graphs are shown in Fig3.25

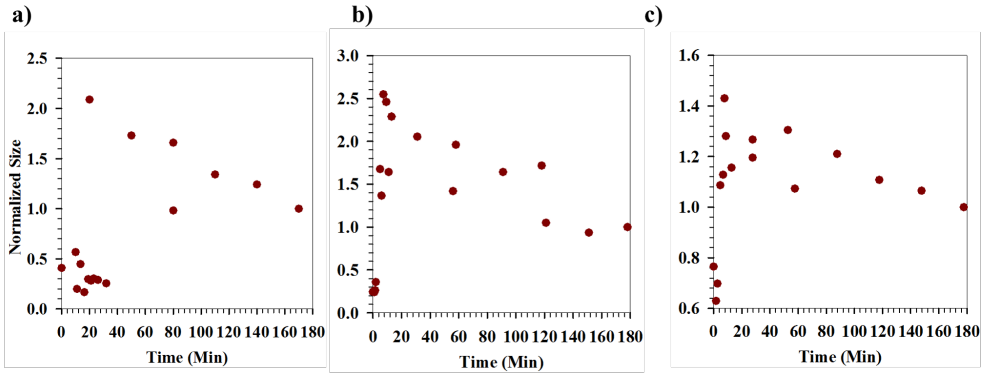


**Figure 3.25:** Normalized size vs Time of NGs synthesized by a) Continuous, b) Flashing and C) Impeller methods.

A common trend of initial increase to maximum and a sudden decrease followed by similar values can be seen in these graphs. The data points do not fit in any curves. Therefore these graphs are also split.

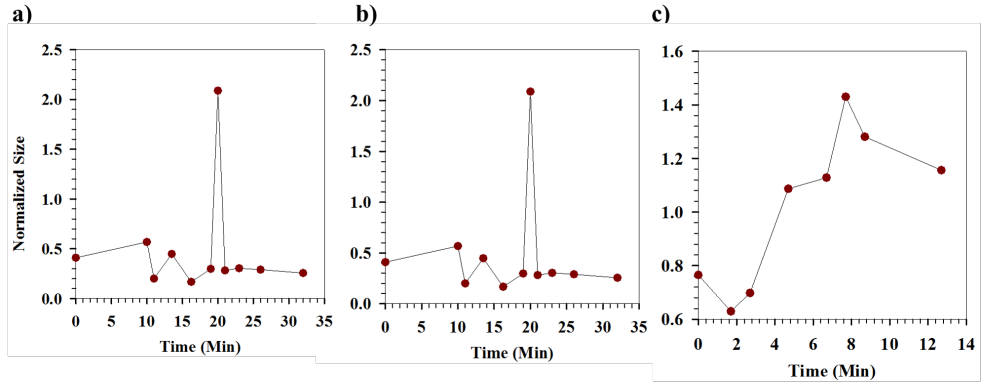


**Figure 3.26:** Normalized size VS Time of NGs synthesized by a) Continuous, b) Flashing and C) Impeller methods.

The normalized data for NG_C vary initially and remains constant. Lack of values around colour change could be the reason for not having a trend. However, NG_F and NG_I follow similar trend. There is an initial stagnation followed by a rapid growth. These look like a sigmoidal growth. Unlike the initial phase, Fig3.27 shows uniform trend for all NGs. There is a linear decrease in size.

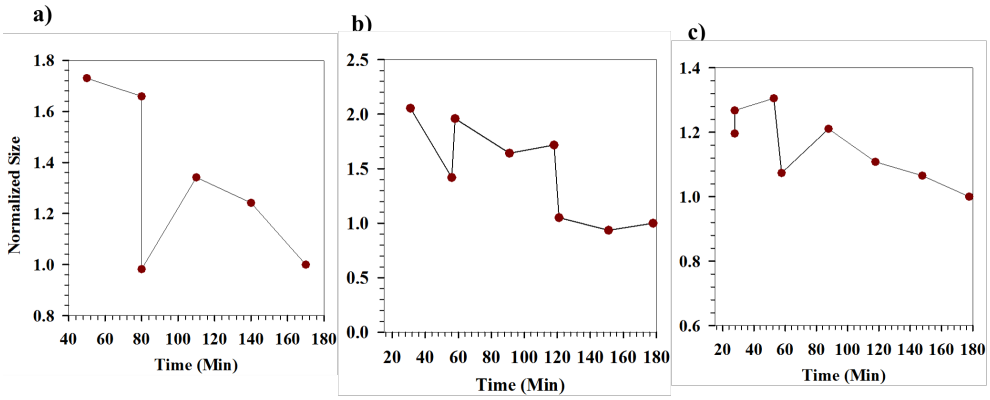


**Figure 3.27:** Normalized size VS Time of NGs synthesized by a) Continuous, b) Flashing and C) Impeller methods.

Sigmoidal curve fits and linear curves fits were used for initial and final phases respectively. The regressions obtained were around 0.88 for initial time period for flashing and impeller method. Linear curve fit was use for the latter part and the regressions were 0.51. 0.71 and 0.68 for NG_C, NG_F and NG_I respectively. These graphs are attached in Appendix D. Although the regression is relatively high for initial phase, it is not observed in continuous method. This could be due to lack of data points around colour change. The regression values are low or there are insufficient data points to analyze these curves. A more detailed analysis of kinetics based these curves is beyond the scope of this thesis.

## 3.6 Growth of NGs

The following observations were made from the timed based study.

- NG_I changes its colour earlier than other NGs.
- Effect of solvent removal has no impact on the final size of NGs.
- VCEs of NGs vary during initial stages of reaction and stabilizes after 60 minutes.
- PDIs of NGs vary a lot and tend to stabilize towards end of the reaction.
- Final PDI of NG_C was lower than the rest.
- VPTT of the NG_C is lower than NG_F and NG_I.

- The size of NGs increases exponentially and then it starts to remain constant around 2 hours.

From these data it is suggested that all NGs grow in a similar trend but they have different kinetics. All the NGs start to grow non-uniformly, and as reaction time proceeds more NGs form. The initial exponential rise in normalized size graphs could be due to the formation and growth of nuclei which can result in very large PDIs. The latter part of the reaction helps the formed NGs to stabilize.

The lack of drastic changes in sizes and PDIs of NG_I suggest that more nuclei are formed immediately after adding the initiator and it has faster kinetics. This could be due to the presence of impeller which could help these NGs to capture oligomers more efficient and start precipitation polymer much earlier than the rest, resulting in a quicker colour change. It can also help stabilizing these nuclei by providing a better access to SDS in the reaction mixture. Alternatively, many nuclei are formed and comparatively little quantity of monomer is available for growth, leading to smaller sizes.

For example, NG_C grow slower than the rest. It is hypothesized that there are lesser nuclei and these grow in to fairly uniform sizes. This is due to availability of more monomers. This can explain lower PDI and its decreasing trend.

NG_F falls in between these two kinetics. The PDI of NG_F slightly increase and the standard deviation of size also increased marginally. However, the collapse remains fairly constant. It is suggested that there is an approximately equal quantity of nuclei and monomers for growth. The competition between forming nuclei and nuclei growth can explain the difference in sizes and PDI of final NGs. This can also explain the constants values of VCE through out the reaction.

From comparing the PDIs and VPTTs of these NGs, it is suggested that monodispersity plays a crucial role in determining VPTT. NGs of similar sizes collapse at one given temperature. However, NGs of different sizes may collapse over a range of temperature and will increase the overall VPTT of the system.

From these analyses, it is hypothesized that NGs does not form uniformly. However, most of the formed nuclei attain their final size with in an hour, the reaction needs to continue to achieve desired collapse and to achieve high monodispersed NGs. However, the sizes and PDIs do not change drastically after 2 hours. Hence it is suggested that the reaction can be stopped after 2 hours. The methods developed to synthesize NGs were used to synthesize hybrid NPs

## 3.7 Hybrid NPs

The flashing and impeller methods developed in Section3.4 were used to synthesize hybrid NPs. Inorganic NPs discussed in section3.1 were used in this process. One major difference in the procedure to synthesize hybrid NPs was the concentration of KPS used. To synthesize bare NGs, 400$\mu$l of 103.5mM KPS was used. However, to synthesize hybrid NPs, the process was optimized and 400$\mu$l of 210mM of KPS was used to initiate the reaction.

In order to compare the sizes and collapses of hybrid NPs, bare NG_F with higher concentration of KPS were synthesized. The synthesized NGs had a size of 233$\pm$ 4nm and VCE was around 89.6%. The size and collapse of this NG will be used as a standard for comparing hybrid NPs size and collapse .

### 3.7.1 Synthesis and Characterization of Hybrid NPs

The procedure to synthesize hybrid NPs is discussed in section 2.3.2. Briefly, NIPAAM, BIS and SDS were mixed and maintained at 70°C. Solution of inorganic NPs at a concentration of 3mg/ml was added and the mixture was stirred. After one hour, AAc and KPS were added. As NGs with desired properties and size can be obtained by 2 hours, the reaction was stopped after 2 hours. SDS was used at a concentration of 4.2mM in all the reactions.

NPs of different shapes,sizes and concentrations were used to synthesize hybrid NPs. Table3.4 shows the list of experiments performed at different concentration of NPs. The reaction mixture turning from colourless to turbid indicated formation of hybrid NPs. This is indicated by 'Y' in Table3.4 and 'N' indicates lack of colour change. The number preceding Y or N refer t the volume of particles solution used. All NPs solution were used at a concentration of 3mg/ml.

| **NPs used** | **Volume of NPs used** | | |
|---|---|---|---|
| Au NS 1 | 0.35-N | 0.5-Y | 1-Y |
| Au NS 2 | 0.35-Y | 0.5-Y | 1-Y |
| Au NS 3 | 0.35-N | 0.5-Y | 1-Y |
| Au NS 4 | 0.35-Y | 0.5-Y | 1-Y |
| Fe@Au | 0.5-Y | 1-Y | 2-Y |

**Table 3.4:** List of experiment performed

Initial experiments with spherical NPs were successful. The characteristic colour change of NGs was observed within few minutes after adding initiator. Presence of inorganic NPs might helps the overall kinetics and the nucleation

switches from being homogeneous to heterogeneous nucleation. In this section, hybrid NPs will be named with the following syntax inorgaicNP used_NG (for example, Au NS1_NG refer to hybrid NP synthesized with Au NS 1). These hybrid NPs had distinct colour similar to that of the inorganic NPs used. This indicates incorporation of inorganic NPs into NGs. For example, hybrid NPs with spherical Au NPs had a pinkish white colour,as shown in Fig3.28.

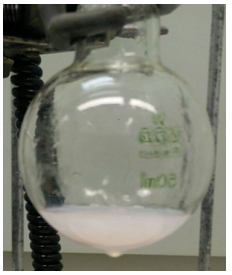

**Figure 3.28:** Pinkish colour of Au NS_NG

These hybrid NPs were dialysed to removes unused chemicals like monomers, extra surfactants. They showed an increase in size after dialysis similar to bare NG.

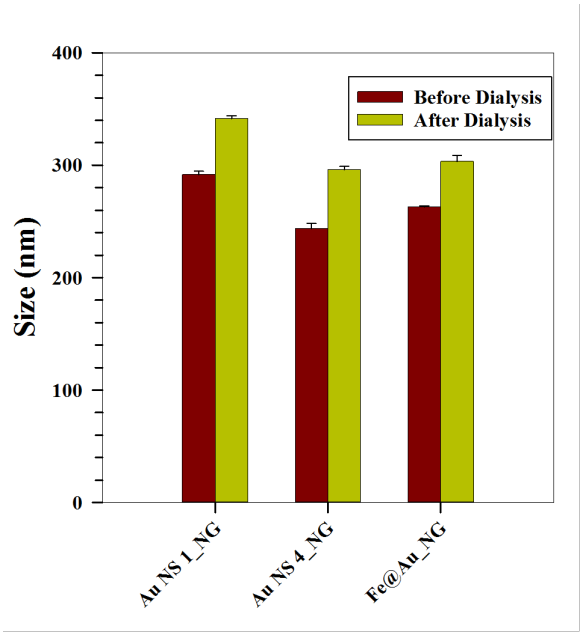


**Figure 3.29:** Representative graph showing the sizes of hybrid NPs before and after dialysis.

Fig3.29 shows a small increase in size after dialysis and this was observed for all hybrid NPs. When comparing the increase in size of hybrid NPs with bare NGs, the extent of increase in size of the hybrid NPs was 17%. This is lower than the 26% that was observed for bare NGs. As mentioned earlier, dialysis removed unused monomers and SDS. The decrease in difference between sizes obtained after and before dialysis suggests that most of NIPAm monomers are being used to form polymers. Presence of inorganic NPs in the reaction mixture might help in achieving better polymerization. This is due to a decrease in Gibbs free energy required for nucleation and growth.

PNIPAm and Au NPs show characteristic absorbance peaks in UV-Vis between 200 and 900nm. In order to check the presence of inorganic NPs and NGs, these hybrid NGs were characterized using UV-Vis. Absorbance values obtained from hybrid NPs were compared against the values of bare NG_F.

Fig3.30a) shows the normalized curves obtained for of bare NG and ER_NG. For each of these curves, absorbance values obtained at each wavelength were normalized against the maximum absorbance obtained. The peaks from ER are visible in the Fig3.30. As inorganic NPs are in NGs, the signals from NGs would interfere with inorganic NPs peaks.

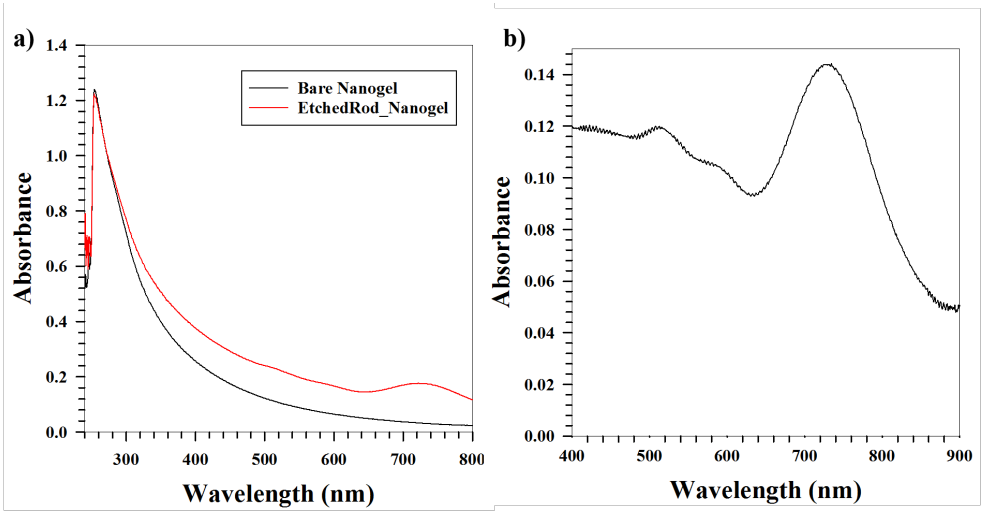


**Figure 3.30:** a)UV-Vis data b)Normalized UV-Vis data.

In order to prevent the interference of polymers in detecting inorganic NPs, a baseline correction was done on the data obtained from these samples. Fig3.30 is a representative image showing baseline corrected absorbance values. The figure

clearly shows the peaks obtained from ER in ER_NG. The peaks obtained are similar to bare NPs peaks. A representative UV-Vis spectra obtained for some of these hybrid NPs are attached in Appendix F

The sizes of these hybrid NPs were higher than the sizes of their corresponding bare NGs or bare NPs. The smallest size of hybrid NPs obtained was 289±4nm. This is still bigger than the biggest bare NG which has a size of 233±4nm. Fig3.31 shows the sizes of largest bare NP used, bare NG along with sizes of few hybrid NPs.

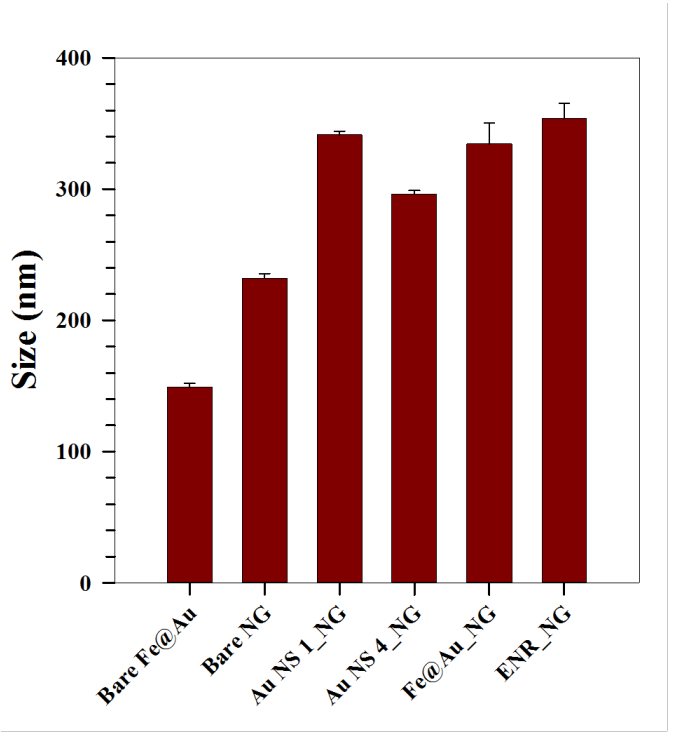


**Figure 3.31:** Comparing sizes of bare NPs, bare NGs and hybrid NPs.

This increase in size shows that inorganic NPs and NGs in hybrid NPs are bound together. In order to check if the binding is strong, hybrid NPs were centrifuged. If the NPs were loosely bound it would leave the polymers as NGs alone could not be precipitated by centrifuging. After centrifuging, a coloured gel like material precipitated, highlighted in Fig3.32. It is suggested that this gel is hybrid NPs without any bare NGs and this showed a 94% collapse. This behaviour suggests a strong binding between NPs and NGs.

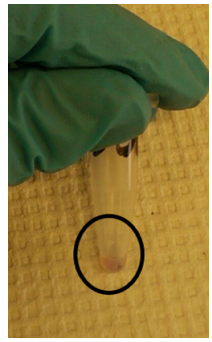

**Figure 3.32:** Hybrid NPs after centrifuging

When measured under UV-Vis, these gel like hybrid NPs showed the LSPR peak only after a baseline correction. This also confirms the presence of NGs after centrifuging.

These samples were observed under S(T)EM to visually check the presence of inorganic NPs. Although these images confirm the presence of inorgaic NPs, the exact location of these NPs cannot be determined. Some representative s(T)EM images are shown in Fig3.33. Inorganic NPs are marked by dark circles and NGs are pointed with red coloured arrows.

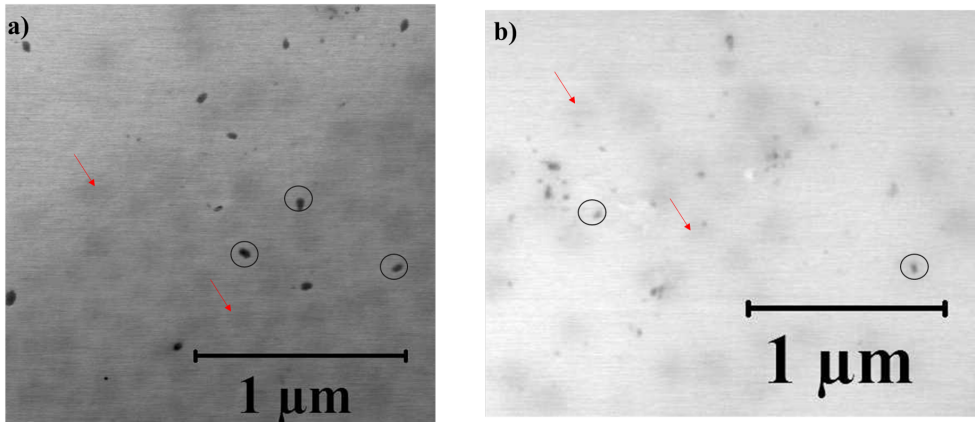


**Figure 3.33:** S(T)EM images of a) AU NS1_NG anf b) AU NS4_NG

In order to understand the effect of inorganic NPs on the physico-chemical properties of the hybrid NPs, different sizes, shapes and concentrations of NPs were used. Effect of surface group was studied by synthesizing hybrid NGs with functionalized NPs. The effect on swelling-collapse of NG was studied by synthesizing Fe@Au_NG by flashing and impeller methods. These are discussed in the

following section.

### 3.7.2 Effect of size

All the measurements shown here onwards were taken after dialysis. Spherical Au NPs and Fe@Au NPs were used to study the effect of size on hybrid NPs. Five different NPs over a range of 100nm were used, with the smallest being 46±4nm and biggest being 150±3nm. Their hydrodynamic sizes are shown in Fig3.34

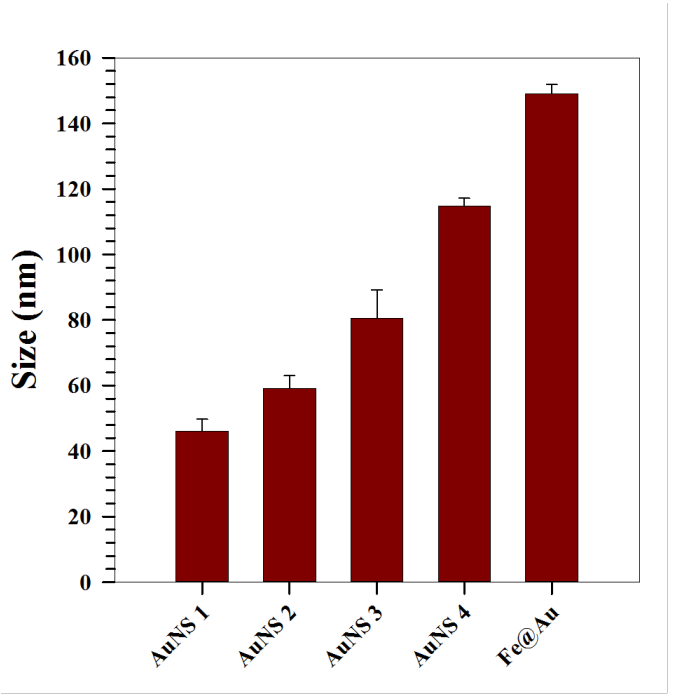


**Figure 3.34:** Spherical NPs used to study the effect of size

In order to check the effect of size, different volumes of NPs were used. One set of experiments was done by using 0.5 ml of inorganic NPs while another set was done with 1ml. This was done to check if the effect of size varies with the number of NPs being added. Fig3.35 shows the sizes of the these NGs at 25°C and 45 °C. X-axis shows the type of inorganic NPs used for synthesizing these hybrid NPs.

Fig3.35 shows that there is almost no effect of size on the size of hybrid NPs when 0.5 ml of inorganic NPs was used. When 1ml of NPs was used, the size decreases slightly and increases and again becomes smaller, as shown in Fig3.35b).

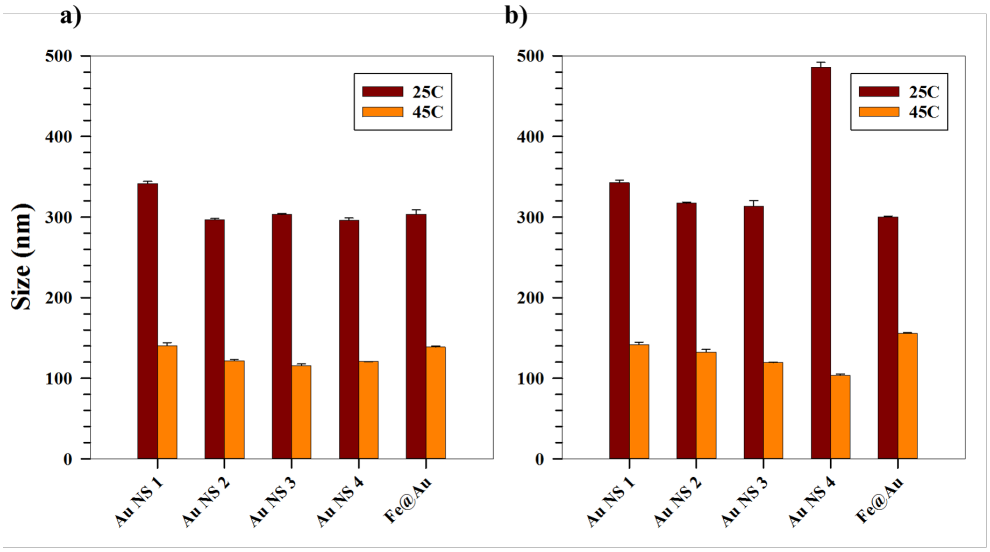


**Figure 3.35:** Effect of size on hybrid NG when a) 500$\mu$l of NP was used b) 1 ml of NPs was used.

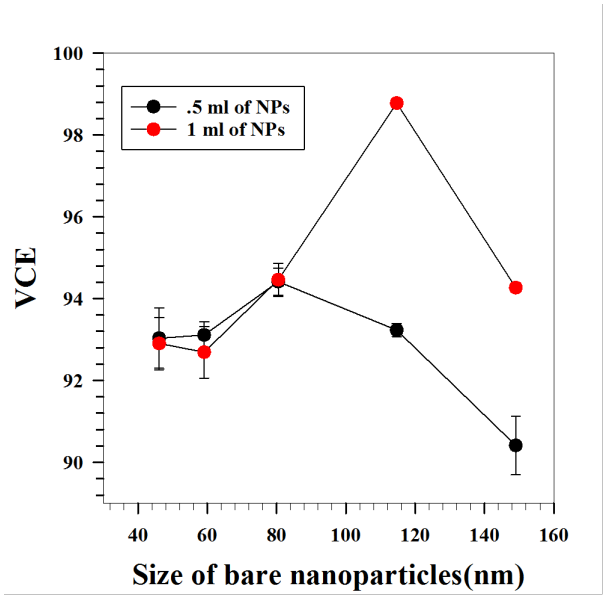


**Figure 3.36:** Effect of size on VCE

The next parameter analyzed is VCE of these hybrid NPs as they can show the impact of inorganic NPs on the collapse behaviour of hybrid NPs. Fig3.36 shows

the VCEs of these hyrbid NPs as a function of the size of their corresponding inorganic NPs. The collapse of hybrid NPs are above 89%, which was the collapse of bare NG. This increase could be due to incorporation of inorganic NPs in the polymeric network. Inorganic NPs may act as cross linker between NGs and help in more efficient collapse.[15]

The VCE increases initially with increase in size and then it starts to decrease. This trend is observed even when different volumes of NPs were used during the experiments. It is suggested that the collapse of hybrid NPs increases until a certain size of NPs after which the collapse decreases, indicating a strong influence of size of inorganic NPs on hybrid NPs.

### 3.7.3 Effect of concentration

#### Spherical Au NPs

Effect of concentration was studied by using different volumes of Au NPs during the start of the reaction. Au NS 2 and Au NS 4 were chosen as these two were prepared by same synthesis routes and had different sizes. Au NS2 was chosen as it was one of the smallest NPs synthesized and Au NS 4 was chosen as it was the biggest Au NS. This comparative study on effect of concentration of these two NPs will help analyze the impact of concentration and size simultaneously. The volumes used were 350$\mu$l, 500$\mu$l and 1ml. The sizes of hybrid NPs at different temperatures are shown in Fig3.37. X axis shows the quantity of Au NPs used to form these hybrid NPs.

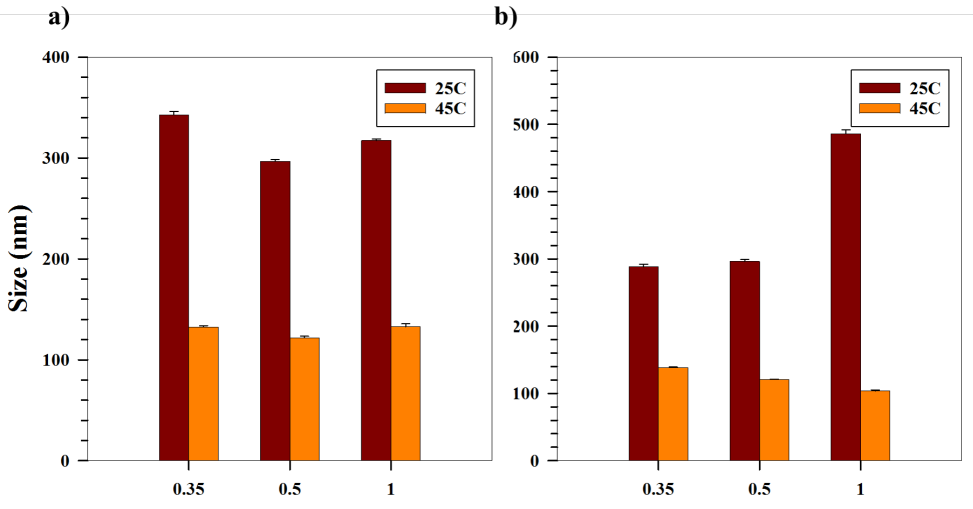


**Figure 3.37:** Effect of Concentration of a)Au NS2 and b)Au NS4.

There is a slight decreasing trend when Au NS2 was used, but there is a steep increase in size when Au NS 4 is used. This difference could be due to the location of these inorganic NPs in the hybrid NGs.

Smaller NPs can easily go inside the NGs. When its concentration is increased, the excess inorganic NPs would go inside the NGs resulting in very small change in the overall size of hybrid NGs. Bigger inorganic NPs might not completely go inside NGs and contribute to the final size of hybrid NPs.

### Fe@Au NPs

Fe@Au NPs were used at 500$\mu$l, 1 ml and 2ml. Similar to Au NS 4, an increase in size of hybrid NPs can be seen in Fig3.38, although the trend is not as profound as Au NS 4.

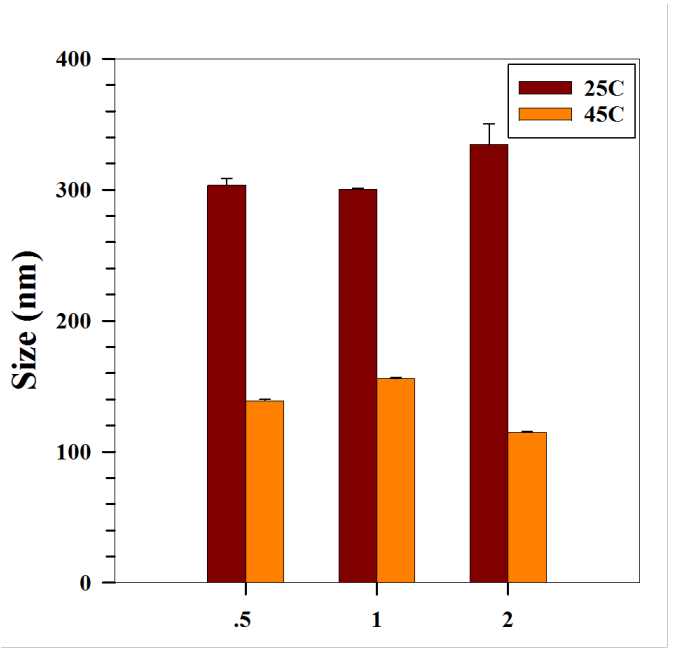


**Figure 3.38:** Effect of Concentration of Fe@Au.

### Effect of concentration on VCE

A plot of VCE against concentration of NPs used is shown in Fig3.39. VCE remains fairly constant for the hybrid NPs containing Au NS2, but it increases with increase in NPs for both Au NS4 and Fe@Au. Effect of concentration is compared with effect of size in Fig3.39.

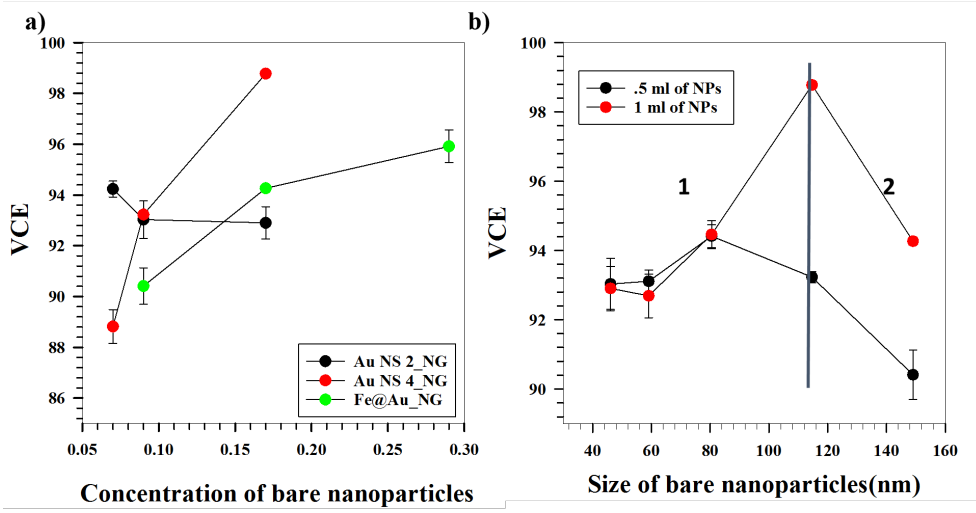


**Figure 3.39:** a)Effect of Concentration on VCE b) Effect of size on VCE

Fig3.39b) can be split into two region. VCE increases in region 1 and decreases in 2. When this is compared with Fig3.39a) it can be inferred that the effect of concentration increases for inorganic NPs that fall in region 2. These results show that concentration has its effect when the size of the NPs used is beyond a certain value. It is hypothesized that location of the inorganic NPs(which is dependent on size) determines the effect of its concentration on hybrid NGs.

### 3.7.4 Effect of shape

From the above discussed experiments, using 500$\mu$l of NPs had consistently produced hybrid NPs. Hence, 500$\mu$l was chosen for synthesizing hybrid NPs with anisotropic NPs. Out of the three NPs used only ER produced desired particles. The size and collapse of the hybrid NGs is compared against Au NP1 and Au NP4 in Fig3.40.The VCE of ER_NG was 93.2%. This is similar to the collapse of of other Au NS1_NG and Au NS4_NG. Despite being anisotropic, impact of ER could be less as its size would fall in the sample region one in VCE vs size plot. During the initial stage of reaction, more nuclei/monomers can interact with ER due to its rugged surface. This could result in ER being captured within the NGs.

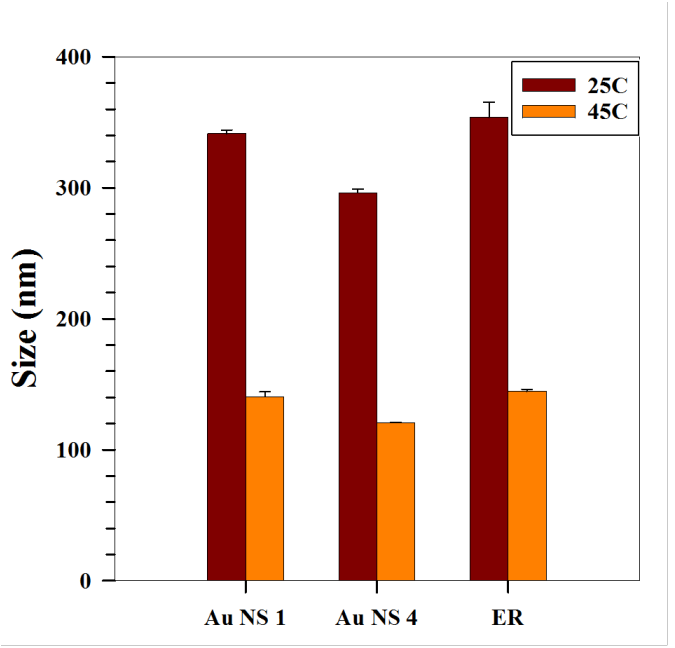


**Figure 3.40:** Effect of Shape

| **Sample** | **VCE** (%) |
|---|---|
| Au NS1_NG | 93.5 ± .74 |
| Au NS4_NG | 93.2 ± .16 |
| ER_NG | 93.2 ±.89 |

**Table 3.5:** VCE of different hybrid NPs

### 3.7.5 Effect of Functional Group

Au NS1 and Au NS4 were separately functionalized with PEG and P-Lysine. These functionalized NPs were used to check the effect of surface charge or surface group on physico-chemical properties of hybrid NPs. PEGylation of the NPs replaces the citrate ligand using a thiol group present in PEG-SH. The physico-chemical properties of these NPs have alrady been discussed in Section3.1.1. Coating with P-Lysine, a cationic ligand, will make the surface of NPs cationic. The sizes of hybrid NPs obtained after functionalization are compared against the hybrid NPs obtained with normal NPs in in Fig3.41. X axis in this figure represents the type of NPs that was used to synthesize the corresponding hybrid NG.

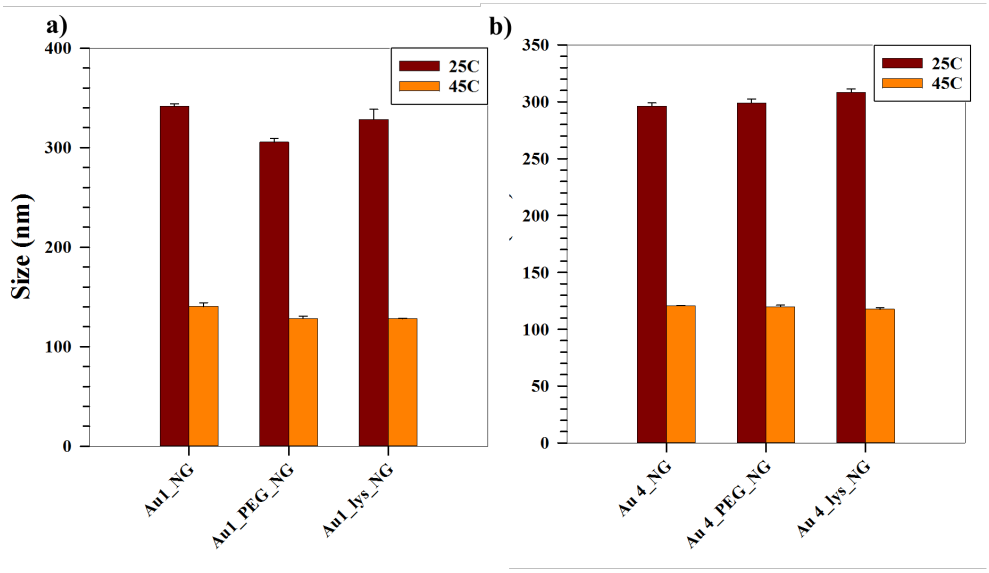


**Figure 3.41:** Effect of functional group of a)Au NS_1 and b) Au NS_4

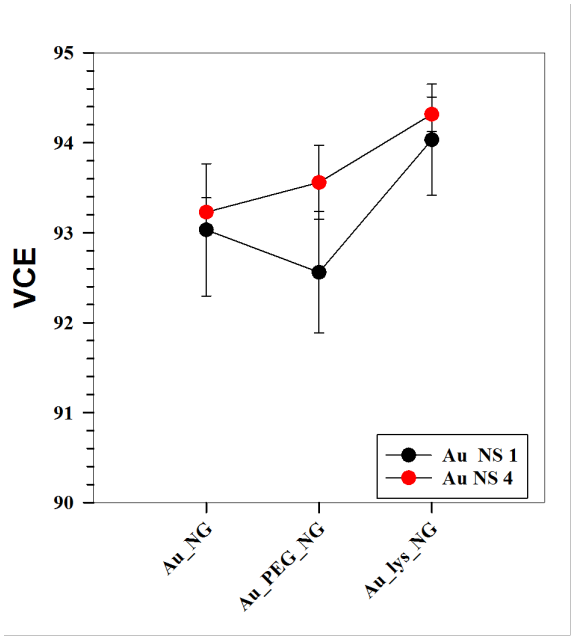


**Figure 3.42:** Effect of functional group on VCE

The effect of functional group on VCE is plotted in Fig3.42. An increase in

VCE can be seen as the surface groups are changed. However, the exact effect of functional group cannot be found from Fig3.42. The sizes of the NPs used to synthesize these hybrid NPs are given in table3.6. These hybrid NPs are plotted according to their sizes given in table3.6, shown in Fig.3.43.

| Nanoparticles | Size (nm) |
|---|---|
| Au NS 1 | $46 \pm 4$ |
| Au NS 1_PEG | $83 \pm 2$ |
| Au NS 1 _PLysine | $123 \pm 8$ |
| Au NS 4 | $115 \pm 3$ |
| Au NS 4_PEG | $138 \pm 2$ |
| Au NS 4 _PLysine | $135 \pm 2$ |

**Table 3.6:** Size of Au NPs

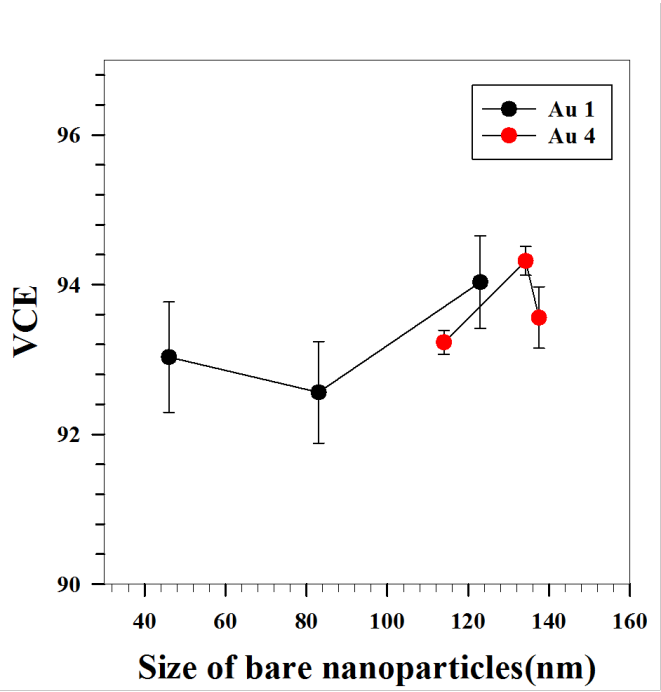


**Figure 3.43:** Effect of size on VCE

The effect of size in Fig3.43 is a bit similar to the trends observed before. The initial increase followed by decrease of VCE is similar, however the decrease is

too less. It is suggested that this variation is caused due to presence of different functional groups on the the surface of inorganic NPs. PEG has a lower molecular weight than P-Lysine.Moreover, at high temperatures PEG is hydrophobic. This might help Au NS 1 to easily enter in to NGs. On the other hand, Au NS1 coated with P-Lysine might be located in the surface of NG and act as a crosslinker, thereby increasing the VCE.

In case of hybrid NPs containing Au NS4, size might play an important role in the location of Au NS4 than the functional group when compared with hybrid NPs containing Au NS1. The decrease in VCE between hybrid NPs with P-Lysine coated Au NS4 and PEG coated Au NS4 could be due to the functional groups on the surface. This can be explained by the hydrophobic interactions between PEG and NGs. Despite being bigger in size, PEG coated Au NS4 could be preferred by NGs and its ability to cross link decreases leading to lesser collapse than the hybrid NPs containing P-Lysine coated Au NS 4.

### 3.7.6 Effect of method of use

Loss of Fe@Au NPs while synthesizing hybrid NPs can be overcome by switching to impeller method. As a preliminary test, 1 ml of Fe@Au NP was used to synthesize hybrid NPs using impeller method(Fe@Au_I_NG). The results obtained were compared against similar experiments done using flashing method(Fe@Au_F_NG). These results are compared against the bare NG_F and NG_I synthesized in Fig3.44.

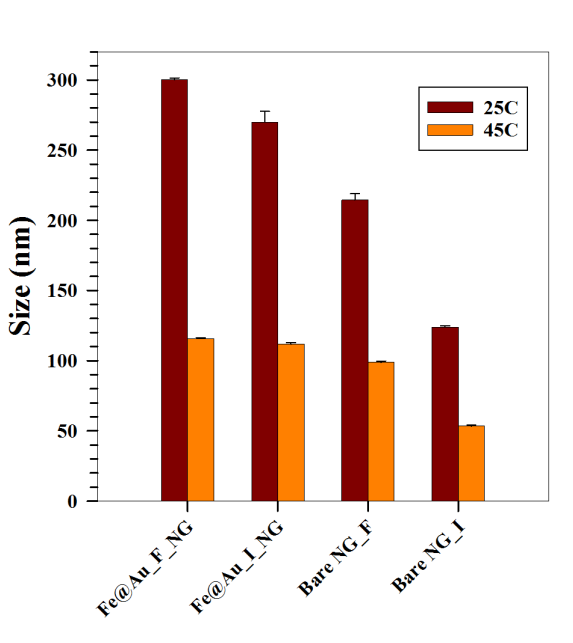


**Figure 3.44:** Effect of Method hybrid NPs and Bare NGs

From Fig3.44, the size of hybrid NPs from impeller method were smaller than the ones from flashing method. This phenomena is also seen in base NGs, also shown in Fig3.44. As shown in Table3.7, there is a small variation in VCE.

| Sample | VCE (%) |
|---|---|
| Fe@Au_F_NG | 94.2 $\pm$.03 |
| Fe@Au_I_NG | 92.9 $\pm$.83 |

**Table 3.7:** VCE of different hybrid NPs

The VCEs of these NPs were almost similar, as shown in Table3.7. This preliminary experiment shows that the impact of changing method on collapse is less. The hybrid NP formed by impeller method had more magnetic properties. These

hybrid NPs can respond to external stimuli like temperature, pH and magnetic field and also be sensed due to the presence of Au, there by helping in synthesizing multifunctional hybrid NPs without significant lose in any of its properties.

## 3.8 VPTT of hybrid NPs

Similar to bare NGs, VPTTs of hybrid NPs were calculated by measuring their sizes at different temperatures. Few of the hybrid NPs were chosen so as to analyze the effects of physical parameters like size and shape on VPTT. VPTT of these are compared against the VPTT of bare NGs and is shown in Table3.8.

| **Hybrid NPs** | **VPTT (°C)** |
|---|---|
| Au NS 1_NG | 36.3 ± .1 |
| Au NS 4_NG | 34.6 ±.05 |
| Au NS 1_PEG | 35.5 ±.05 |
| AU NS 4_PEG | 34.9 ±.07 |
| ER_NG | 34.9 ± .05 |
| Fe@Au_F_NG | 34.9 ± .06 |
| Fe@Au_MS_NG | 35.4± .05 |
| Bare NG_F | 37.8 ±.1 |
| Bare NG_I | 37.7 ± .1 |

**Table 3.8:** VPTT of different hybrid NPs

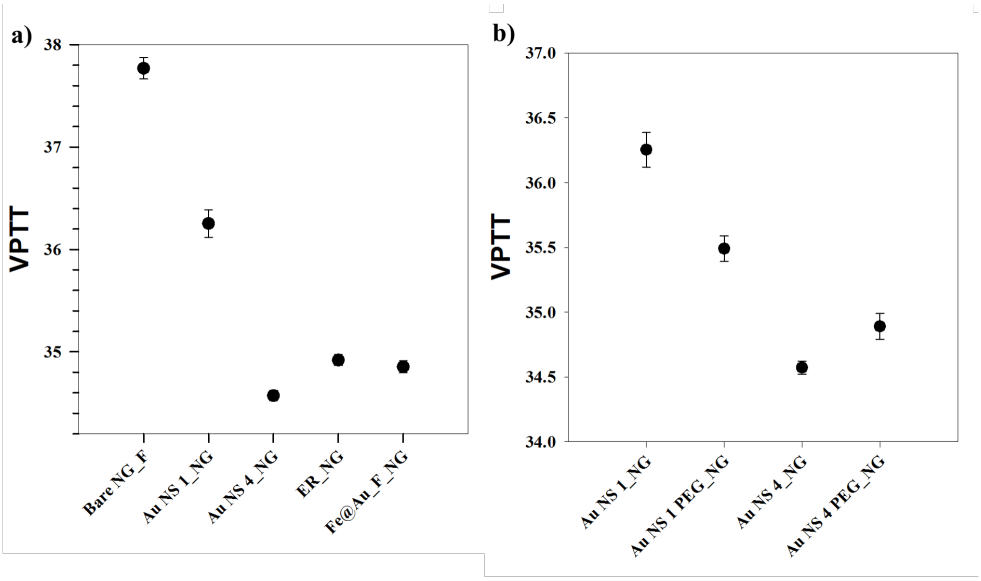


**Figure 3.45:** VPTT of bare and hybrid NPs

Figs 3.45a) and Table 3.8 show that hybrid NPs has lower VPTT than their

corresponding bare NGs and bigger inorganic NPs have lower VPTT. VPTT of Au NS1_NG is highest of all the hybrid NPs. This suggests that bigger NPs help in overall collapse of the hybrid NPs than the smaller ones.

The effect of functional group was studied by comparing AuNS1_NG and AuNS4_NG with their PEG coated counterparts and is shown in Fig 3.45b). There is a decrease in VPTT for Au NS1_PEG_NG, this could be due to the hydrophobic interactions of PEG, as discussed in Section 3.7.5 . However this phenomenon is not seen in Au NS4_PEG_NG as these are bigger and could be on the surface of NGs. This would lead to increase in collapse as observed in Section 3.7.5.

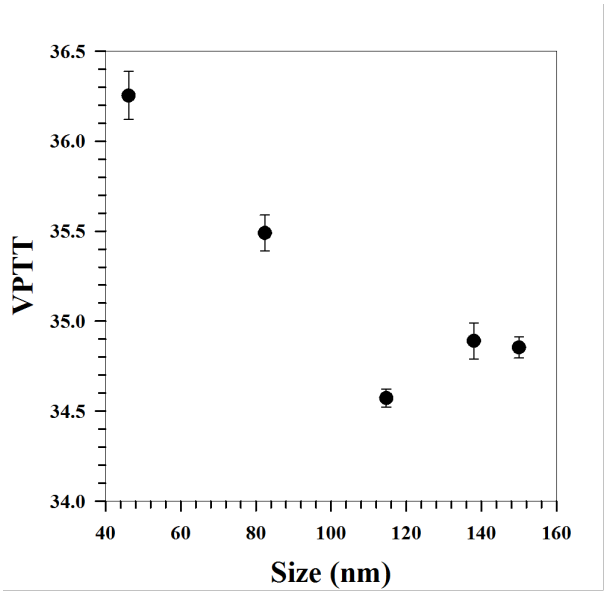


**Figure 3.46:** VPTT of bare and hybrid NPs

Fig 3.46 shows the VPTT dependence on size of inorganic NPs used. VPTT is higher for smaller inorganic NPs and it start to decrease with increase in size up to a certain point, after which it starts to increase a little. The initial decrease in VPTT could due to increase in cross linking ability of the bigger inorganic NP. However, after a certain size NPs start to aggregate among themselves at higher temperature and might not contribute to the collapse of the hybrid NPs.

Based on the effect of size, shape and concentration of inorganic NPs that were discussed, it is suggested that the location of these NPs in hybrid NPs may vary. This variation depends on the size of the inorganic NPs used and these variations directly impacts the VPTT of these hybrid NPs.

## 3.9 Morphology of Hybrid NPs

Based on the data obtained by characterizing the hybrid NPs, the interaction between inorganic NPs and NGs in hybrid NPs could be one of the following

- NGs grow on top inorganic of NPs.
- Surface of inorganic NPs is shared between NGs.
- NGs are captured by several NPs, forming a ring like arrangement around NGs
- NPs are bound in a matrix of NGs.
- NPs are captured by NGs

From analyzing the hybrid NPs and studying the effect of size, shape, concentration of inorganic NPs, the following observations and inferences were made

- Size of hybrid NPs increase after dialysis.
- The colour from NPs used were visible in hybrid NPs.
- Absorbance peak from PNIPAm did not change after incorporation of inorganic NPs.
- LSPR peaks of Au NPs were visible after a baseline correction.
- Hybrid NPs obtained after centrifuging behave similarly to the ones before centrifuging.
- Hybrid NGs were bigger than bare NPs and NGs.
- Size of inorganic NPs affects the VCE of hybrid NPs.
- Effect of concentration depends on size of inorganic NPs.
- Functional group on the surface of inorganic NPs affect the collapse of hybrid NPs.
- Hybrid NPs from impeller method was smaller than similar NGs synthesized from flashing method
- VPTT was affected by size, shape of NG and the method used.
- Location of inorganic NPs depend on its size.

It is hypothesized that depending on the size of NPs, they are either fully or partially captured by NGs while forming hybrid NPs. When smaller inorganic NPs are used, some of them are completely inside the NGs and some are on the surface of NGs. This is illsustated in Fig3.47.

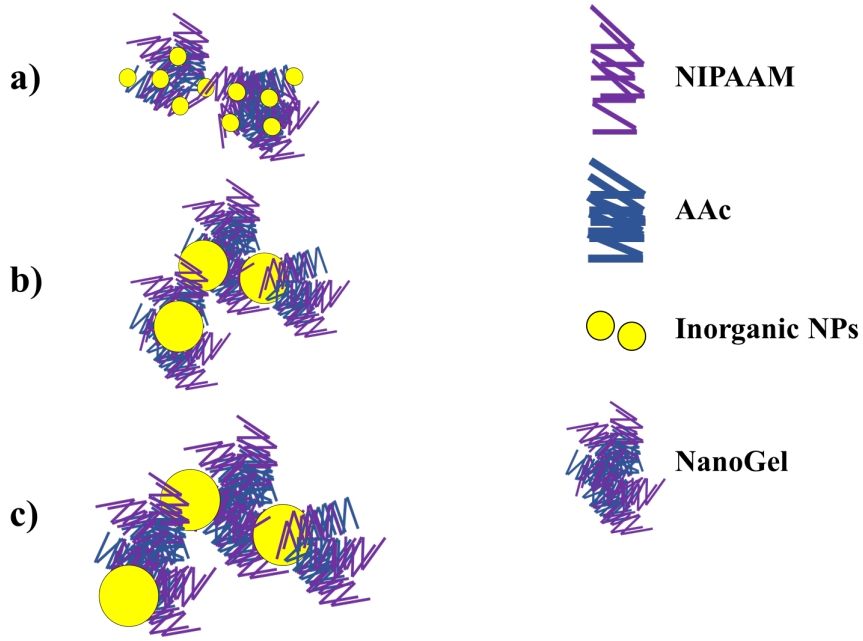


**Figure 3.47:** Inorganic NPs size dependent structure of hybrid NPs

Fig 3.47 a),b) and c) show the morphology of hybrid NPs synthesized with small, medium and big inorganic NPs respectively. As the size of inorganic NP increases, the number of inorganic NPs captured decreases and big particles are partially captured or shared between two or more NGs. Bigger inorganic NPs are predominantly on the surface of NGs. The particles on the surface of NGs act as a cross-linker between NGs. This assembly of inorganic NPs leads to decrease in VPTT of hybrid NPs. The cross-linking of NGs by NPs, help it to collapse more efficiently thereby decreasing the VPTT. The variations in VPTT between hybrid NPs depend on the sizes and functional group of the inorganic NPs used

When concentration of smaller inorganic NPs is increased, there is no effect on collapse as most of them will be captured by other NGs in the system[3]. On the other hand, the collapse will increase when more inorganic NPs are used if they are bigger in size. This is due to more effective cross-linking by these inorganic

[3] As discussed earlier, bare NGs will also form along with hybrid NGs

NPs.

As the size of inorganic NPs increases, the collapse or VCE increases because the NPs start to cross-link. After a certain size, the NPs that now act as cross-linker will start to aggregate and the competition between inorganic NPs aggregation and collapse of NGs might cause the reduction in VCE at higher size.

In short, the location of the inorganic NPs used to synthesize hybrid NPs determine its physico-chemical properties. The location of inorganic NPs depends on its size and effect of parameters such as concentration and surface functional group are also dependent on the size. The VCE and VPTT, two most important properties of hybrid NPs, can be altered by changing the size of the inorganic NPs used.

Chapter 4

# Conclusion

The study focused on synthesizing polymeric and hybrid NPs using different methods with an aim to modify thier physico-chemical properties. Several inorganic, polymeric and hybrid NPs were synthesized for this study. These were characterized and their behaviour were studied by using DLS, UV-Vis and S(T)EM.

Inorganic NPs of Fe and Au were synthesized by a number of different synthesis routes. Different sizes of spherical Au NPs and different shapes of Au NPs, such as nanorod, etched rod and nanomakura, were synthesized. Spherical Au NPs were also functionalized with PEG or P-Lysine. These NPs were used for synthesizing hybid NPs.

Polymeric NPs of PNIPAM/AAc of different sizes were synthesized and characterized. These NPs were synthesized under nitrogen atmosphere for the entire reaction period. Two alternate methods, flashing and impeller method, were used to synthesize similar polymeric NPs. The NPs synthesized from these three methods were compared. The swelling-collapse of these NPs compared and it was found that NPs synthesized from flashing and mechanical stirring showed a volumetric collapse efficiency around 90% at all concentration of SDS used, where as it dropped to 44% for NPs produced by continuous method when 2.1mM of SDS was used.

Flashing and stirring method produces NGs of different sizes but with similar collapse. The smallest NGs produced by these methods was around $128\pm2$nm and the largest NGs had a size of $373\pm4$nm. The methods reduced the quantity of nitrogen used in the reaction by reducing the need for nitrogen atmosphere from 4 hours to 5 minutes. The overall time required to achieve the desired NGs after

initiating the reaction was also reduced from 3 hours to 2 hours. The impeller method helps in achieving the final size much quicker than the other method. In impeller method, replacing magnetic stirrer with impeller allows it to be used in reactions that involve magnetic NPs. Impeller method ensures no loss of NPs in such scenarios.

VPTTs of these NPs were determined by tracking the variation in sizes of these NPs with respect to temperature. The VPTTs of NPs synthesized by continuous, flashing and impeller methods were 36.4°C, 37.8°c and 37.7°C respectively. The growth of these NPs were studied and it was suggested that all these NPs grow similarly but the kinetics of these reactions vary.

The process to synthesize hybrid NPs was optimized and the hybrid NPs obtained were compared against bare polymeric NPs. Different techniques were used to check the binding of inorganic NPs with polymeric NPs. Effects of size, shape and concentration of inorganic NP were studied. It was hypothesized that size plays an important role in swelling-collapse property of these hybrid NPs. Flashing and impeller methods were used to synthesize hybrid NPs and their effect were studied. The VCE of hybrid NPs synthesized by these methods were 94.2±.03% and 92.9±.83 %. VPTT was calculated for these hybrid NPs.

Of all the hybrid NPs, the ones synthesized using Au NS4 has the maximum collapse. It collapsed from 487±6 nm to 104±2nm with a 98.7±.01% VCE. A maximum of 95.9±.4% of VCE was achieved while using Fe@Au NPs. Hybrid NPs with bigger inorganic NPs had lower VPTT and it was hypothesized that bigger inorganic NPs helped in collapse.The maximum VPTT obtained was 36.3 ±.2 °C for hybrid NPs synthesized with Au NS1 and the minimum VPTT was 346±.1°C for hybrid NPs synthesized with Au NS4.

From the results obtained it was hypothesized that physico-chemical properties of hybrid NPs depend on the size of the inorganic NPs used. Smaller particles are completely inside the NGs with few on the surface of NGs. On the other hand, bigger particles tend to be on the surface and act as cross linker between NGs. Bigger the size of the inorganic NPs, higher its ability to cross link. These cross links help in overall collapse of the hybrid NPs and reduces the VPTT of such hybrid NPs.

Chapter 5

# Future Work

Successful synthesis of multifunctional hybrid NPs was shown in this work, the growth of the hybrid NPs can be studied to understand them better. The effect of shape on hybrid NPs can be studied extensively. Various other functional groups can be used to study their individual effects. Similar experiments can be performed for impeller method to study the effect of size, shape and concentration of magnetic and other NPs. The results from these can be compared with effect of these parameters when similar experiments are performed with flashing and continuous methods.

The hybrid NPs can be loaded with drug and loading and release studies can be done. These can also be used to encapsulate biomolecules like DNAs,siRNA among other things. More time based experiments of bare NGs and hybrid NGs can be performed to determine the kinetics of these.A preliminary study comparing size dependence on collapse and VPTT was preformed. An extensive study can help build a predictive model which can be used to determine the physico-chemical properties of hybrid NPs with the knowledge of sizes of inorganic NPs used.

# Bibliography


[1] Philip D Howes, Rona Chandrawati, and Molly M Stevens. Colloidal nanoparticles as advanced biological sensors. *Science*, 346(6205):1247390, 2014.

[2] Saji Alex and Ashutosh Tiwari. Functionalized gold nanoparticles: synthesis, properties and applicationsa review. *Journal of nanoscience and nanotechnology*, 15(3):1869–1894, 2015.

[3] Rishikesh M Sawant, JP Hurley, S Salmaso, A Kale, E Tolcheva, TS Levchenko, and VP Torchilin. smart drug delivery systems: double-targeted ph-responsive pharmaceutical nanocarriers. *Bioconjugate chemistry*, 17(4):943–949, 2006.

[4] Igor L Medintz, H Tetsuo Uyeda, Ellen R Goldman, and Hedi Mattoussi. Quantum dot bioconjugates for imaging, labelling and sensing. *Nature materials*, 4(6):435–446, 2005.

[5] Akiyoshi Hoshino, Noriyoshi Manabe, Kouki Fujioka, Kazuo Suzuki, Masato Yasuhara, and Kenji Yamamoto. Use of fluorescent quantum dot bioconjugates for cellular imaging of immune cells, cell organelle labeling, and nanomedicine: surface modification regulates biological function, including cytotoxicity. *Journal of Artificial Organs*, 10(3):149–157, 2007.

[6] Xiaohua Huang, Prashant K Jain, Ivan H El-Sayed, and Mostafa A El-Sayed. Gold nanoparticles: interesting optical properties and recent applications in cancer diagnostics and therapy. *Nanomedicine*, 2(5):681–693, 2007.

[7] An-Hui Lu, E emsp14L Salabas, and Ferdi Schüth. Magnetic nanoparticles: synthesis, protection, functionalization, and application. *Angewandte Chemie International Edition*, 46(8):1222–1244, 2007.

[8] Nuria Sanvicens and M Pilar Marco. Multifunctional nanoparticles–properties and prospects for their use in human medicine. *Trends in biotechnology*, 26(8):425–433, 2008.

[9] Monty Liong, Jie Lu, Michael Kovochich, Tian Xia, Stefan G Ruehm, Andre E Nel, Fuyuhiko Tamanoi, and Jeffrey I Zink. Multifunctional inorganic nanoparticles for imaging, targeting, and drug delivery. *ACS nano*, 2(5):889–896, 2008.

[10] Hyeonseok Yoon and Jyongsik Jang. Conducting-polymer nanomaterials for high-performance sensor applications: issues and challenges. *Advanced Functional Materials*, 19(10):1567–1576, 2009.

[11] Jaemoon Yang, Choong-Hwan Lee, Hyun-Ju Ko, Jin-Suck Suh, Ho-Geun Yoon, Kwangyeol Lee, Yong-Min Huh, and Seungjoo Haam. Multifunctional magneto-polymeric nanohybrids for targeted detection and synergistic therapeutic effects on breast cancer. *Angewandte Chemie International Edition*, 46(46):8836–8839, 2007.

[12] Chenjie Xu, Jin Xie, Don Ho, Chao Wang, Nathan Kohler, Edward G Walsh, Jeffrey R Morgan, Y Eugene Chin, and Shouheng Sun. Au–fe3o4 dumbbell nanoparticles as dual-functional probes. *Angewandte Chemie*, 120(1):179–182, 2008.

[13] Nicole Glaser, Dave J Adams, Alexander Böker, and Georg Krausch. Janus particles at liquid- liquid interfaces. *Langmuir*, 22(12):5227–5229, 2006.

[14] Sulalit Bandyopadhyay. *Smart and multifunctional core-shell nanoparticles for drug delivery*. PhD thesis, 2016.

[15] Sulalit Bandyopadhyay, Marte Kee Andersen, Muhammad Awais Ashfaq Alvi, Anuvansh Sharma, Rajesh Raju, Birgitte H McDonagh, and Wilhelm Robert Glomm. Incorporation of fe@ au nanoparticles into multiresponsive pnipam-aac colloidal gels modulates drug uptake and release. *Colloid and Polymer Science*, 294(12):1929–1942, 2016.

[16] Mani Ethayaraja, Chettiannan Ravikumar, Devarajan Muthukumaran, Kanchan Dutta, and Rajdip Bandyopadhyaya. Cds- zns core- shell nanoparticle formation: Experiment, mechanism, and simulation. *The Journal of Physical Chemistry C*, 111(8):3246–3252, 2007.

[17] T Jafari, A Simchi, and N Khakpash. Synthesis and cytotoxicity assessment of superparamagnetic iron–gold core–shell nanoparticles coated with polyglycerol. *Journal of colloid and interface science*, 345(1):64–71, 2010.

[18] Dong Chen, Jiajun Li, Chunsheng Shi, Xiwen Du, Naiqin Zhao, Jing Sheng, and Shuo Liu. Properties of core- shell ni- au nanoparticles synthesized through a redox-transmetalation method in reverse microemulsion. *Chemistry of materials*, 19(14):3399–3405, 2007.

[19] HPFD Fessi, François Puisieux, J Ph Devissaguet, Nicolas Ammoury, and Simon Benita. Nanocapsule formation by interfacial polymer deposition following solvent displacement. *International journal of pharmaceutics*, 55(1):R1–R4, 1989.

[20] Federica Lince, Daniele L Marchisio, and Antonello A Barresi. Strategies to control the particle size distribution of poly-$\varepsilon$-caprolactone nanoparticles for pharmaceutical applications. *Journal of Colloid and Interface Science*, 322(2):505–515, 2008.

[21] Anatolii D Pomogailo and Vladimir N Kestelman. Chemical methods of metal-polymer nanocomposite production. *Metallopolymer Nanocomposites*, pages 135–236, 2005.

[22] Lavinia Balan and Dominique Burget. Synthesis of metal/polymer nanocomposite by uv-radiation curing. *European Polymer Journal*, 42(12):3180–3189, 2006.

[23] Wael H Eisa, Yasser K Abdel-Moneam, AAM Shabaka, and Abd El-Hameed M Hosam. In situ approach induced growth of highly monodispersed ag nanoparticles within free standing pva/pvp films. *Spectrochimica Acta Part A: Molecular and Biomolecular Spectroscopy*, 95:341–346, 2012.

[24] Sarita Kango, Susheel Kalia, Annamaria Celli, James Njuguna, Youssef Habibi, and Rajesh Kumar. Surface modification of inorganic nanoparticles for development of organic–inorganic nanocompositesa review. *Progress in Polymer Science*, 38(8):1232–1261, 2013.

[25] Cheng Guan, Changli Lü, Yuanrong Cheng, Shouyin Song, and Bai Yang. A facile one-pot route to transparent polymer nanocomposites with high zns nanophase contents via in situ bulk polymerization. *Journal of Materials Chemistry*, 19(5):617–621, 2009.

[26] SS Park, N Bernet, S De La Roche, and HT Hahn. Processing of iron oxide-epoxy vinyl ester nanocomposites. *Journal of Composite Materials*, 37(5):465–476, 2003.

[27] Zdravka Medarova, Wellington Pham, Christian Farrar, Victoria Petkova, and Anna Moore. In vivo imaging of sirna delivery and silencing in tumors. *Nature medicine*, 13(3):372–377, 2007.

[28] Mani Ethayaraja and Rajdip Bandyopadhyaya. Model for core- shell nanoparticle formation by ion-exchange mechanism. *Industrial & Engineering Chemistry Research*, 47(16):5982–5985, 2008.

[29] Tae-Jong Yoon, Jun Sung Kim, Byung Geol Kim, Kyeong Nam Yu, Myung-Haing Cho, and Jin-Kyu Lee. Multifunctional nanoparticles possessing a magnetic motor effect for drug or gene delivery. *Angewandte Chemie*, 117(7):1092–1095, 2005.

[30] Nynke AM Verhaegh and Alfons van Blaaderen. Dispersions of rhodamine-labeled silica spheres: synthesis, characterization, and fluorescence confocal scanning laser microscopy. *Langmuir*, 10(5):1427–1438, 1994.

[31] Alfons Van Blaaderen and A Vrij. Synthesis and characterization of colloidal dispersions of fluorescent, monodisperse silica spheres. *Langmuir*, 8(12):2921–2931, 1992.

[32] Hadi M Zareie, Cyrille Boyer, Volga Bulmus, Ebrahim Nateghi, and Thomas P Davis. Temperature-responsive self-assembled monolayers of oligo (ethylene glycol): control of biomolecular recognition. *Acs Nano*, 2(4):757–765, 2008.

[33] Habib Skaff and Todd Emrick. The use of 4-substituted pyridines to afford amphiphilic, pegylated cadmium selenide nanoparticles. *Chemical Communications*, (1):52–53, 2003.

[34] Shyh-Dar Li and Leaf Huang. Stealth nanoparticles: high density but sheddable peg is a key for tumor targeting. *Journal of controlled release: official journal of the Controlled Release Society*, 145(3):178, 2010.

[35] Prashant K Jain, Xiaohua Huang, Ivan H El-Sayed, and Mostafa A El-Sayed. Noble metals on the nanoscale: optical and photothermal properties and some applications in imaging, sensing, biology, and medicine. *Accounts of chemical research*, 41(12):1578–1586, 2008.

[36] Erik C Dreaden and Mostafa A El-Sayed. Detecting and destroying cancer cells in more than one way with noble metals and different confinement properties on the nanoscale. *Accounts of chemical research*, 45(11):1854–1865, 2012.

[37] Susie Eustis and Mostafa A El-Sayed. Why gold nanoparticles are more precious than pretty gold: noble metal surface plasmon resonance and its enhancement of the radiative and nonradiative properties of nanocrystals of different shapes. *Chemical society reviews*, 35(3):209–217, 2006.

[38] Jian You, Rui Zhang, Guodong Zhang, Meng Zhong, Yang Liu, Carolyn S Van Pelt, Dong Liang, Wei Wei, Anil K Sood, and Chun Li. Photothermal-chemotherapy with doxorubicin-loaded hollow gold nanospheres: A platform for near-infrared light-trigged drug release. *Journal of controlled release*, 158(2):319–328, 2012.

[39] Adam M Schwartzberg, Tammy Y Olson, Chad E Talley, and Jin Z Zhang. Synthesis, characterization, and tunable optical properties of hollow gold nanospheres. *The Journal of Physical Chemistry B*, 110(40):19935–19944, 2006.

[40] C Wilhelm, C Billotey, J Roger, JN Pons, J-C Bacri, and F Gazeau. Intracellular uptake of anionic superparamagnetic nanoparticles as a function of their surface coating. *Biomaterials*, 24(6):1001–1011, 2003.

[41] Yong Wang, Jian Feng Wong, Xiaowei Teng, Xue Zhang Lin, and Hong Yang. pulling nanoparticles into water: phase transfer of oleic acid stabilized monodisperse nanoparticles into aqueous solutions of $\alpha$-cyclodextrin. *Nano Letters*, 3(11):1555–1559, 2003.

[42] Mahmoud Elsabahy and Karen L Wooley. Design of polymeric nanoparticles for biomedical delivery applications. *Chemical Society Reviews*, 41(7):2545–2561, 2012.

[43] William Leobandung, Hideki Ichikawa, Yoshinobu Fukumori, and Nicholas A Peppas. Monodisperse nanoparticles of poly (ethylene glycol) macromers and n-isopropyl acrylamide for biomedical applications. *Journal of Applied Polymer Science*, 87(10):1678–1684, 2003.

[44] Michael Heskins and James E Guillet. Solution properties of poly (n-isopropylacrylamide). *Journal of Macromolecular ScienceChemistry*, 2(8):1441–1455, 1968.

[45] Satish Nayak and L Andrew Lyon. Soft nanotechnology with soft nanoparticles. *Angewandte chemie international edition*, 44(47):7686–7708, 2005.

[46] Yogesh B Patil, Udaya S Toti, Ayman Khdair, Linan Ma, and Jayanth Panyam. Single-step surface functionalization of polymeric nanoparticles for targeted drug delivery. *Biomaterials*, 30(5):859–866, 2009.

[47] William H Blackburn, Erin B Dickerson, Michael H Smith, John F McDonald, and L Andrew Lyon. Peptide-functionalized nanogels for targeted sirna delivery. *Bioconjugate chemistry*, 20(5):960–968, 2009.

[48] Kumaresh S Soppimath, L-H Liu, Wei Yang Seow, S-Q Liu, Ross Powell, Peggy Chan, and Yi Yan Yang. Multifunctional core/shell nanoparticles self-assembled from ph-induced thermosensitive polymers for targeted intracellular anticancer drug delivery. *Advanced Functional Materials*, 17(3):355–362, 2007.

[49] Sulalit Bandyopadhyay, Gurvinder Singh, Ioanna Sandvig, Axel Sandvig, Roland Mathieu, P Anil Kumar, and Wilhelm Robert Glomm. Synthesis and in vitro cellular interactions of superparamagnetic iron nanoparticles with a crystalline gold shell. *Applied Surface Science*, 316:171–178, 2014.

[50] Jun Liu, Robert Pelton, and Andrew N Hrymak. Properties of poly (n-isopropylacrylamide)-grafted colloidal silica. *Journal of colloid and interface science*, 227(2):408–411, 2000.

[51] Xiaofeng Liu, Mei Zhu, Songhua Chen, Mingjian Yuan, Yanbing Guo, Yinglin Song, Huibiao Liu, and Yuliang Li. Organic- inorganic nanohybrids via directly grafting gold nanoparticles onto conjugated copolymers through the diels- alder reaction. *Langmuir*, 24(20):11967–11974, 2008.

[52] Dawei Huang, Chenggang Niu, Xiaoyu Wang, Xiaoxiao Lv, and Guangming Zeng. turn-on fluorescent sensor for hg2+ based on single-stranded dna functionalized mn: Cds/zns quantum dots and gold nanoparticles by time-gated mode. *Analytical chemistry*, 85(2):1164–1170, 2013.

[53] Melgardt M De Villiers, Pornanong Aramwit, and Glen S Kwon. *Nanotechnology in drug delivery*. Springer Science & Business Media, 2008.

[54] M Chese, R Yang, E Hubbell, A Berno, XC Huang, D Stern, et al. Accessing genetic information with high-density dna array. *Science*, 224:610–14, 1996.

[55] Cristian Staii, Alan T Johnson, Michelle Chen, and Alan Gelperin. Dna-decorated carbon nanotubes for chemical sensing. *Nano Letters*, 5(9):1774–1778, 2005.

[56] Michela Puddu, Daniela Paunescu, Wendelin J Stark, and Robert N Grass. Magnetically recoverable, thermostable, hydrophobic dna/silica encapsulates and their application as invisible oil tags. *ACS nano*, 8(3):2677–2685, 2014.

[57] Hongjie An and Bo Jin. Prospects of nanoparticle–dna binding and its implications in medical biotechnology. *Biotechnology advances*, 30(6):1721–1732, 2012.

[58] Rongchao Jin, Guosheng Wu, Zhi Li, Chad A Mirkin, and George C Schatz. What controls the melting properties of dna-linked gold nanoparticle assemblies? *Journal of the American Chemical Society*, 125(6):1643–1654, 2003.

[59] AB Steel, RL Levicky, TM Herne, and Michael J Tarlov. Immobilization of nucleic acids at solid surfaces: effect of oligonucleotide length on layer assembly. *Biophysical journal*, 79(2):975–981, 2000.

[60] Brent S Gaylord, Alan J Heeger, and Guillermo C Bazan. Dna detection using water-soluble conjugated polymers and peptide nucleic acid probes. *Proceedings of the National Academy of Sciences*, 99(17):10954–10957, 2002.

[61] Michael H Smith and L Andrew Lyon. Multifunctional nanogels for sirna delivery. *Accounts of chemical research*, 45(7):985–993, 2011.

[62] Yong Zhang, Nathan Kohler, and Miqin Zhang. Surface modification of superparamagnetic magnetite nanoparticles and their intracellular uptake. *Biomaterials*, 23(7):1553–1561, 2002.

[63] Xianjia Peng, Zhaokun Luan, Jun Ding, Zechao Di, Yanhui Li, and Binghui Tian. Ceria nanoparticles supported on carbon nanotubes for the removal of arsenate from water. *Materials letters*, 59(4):399–403, 2005.

[64] Jan Kostal, Giridhar Prabhukumar, U Loi Lao, Alin Chen, Mark Matsumoto, Ashok Mulchandani, and Wilfred Chen*. Customizable biopolymers for heavy metal remediation. *Journal of Nanoparticle Research*, 7(4):517–523, 2005.

[65] Chao Wang, Hongfeng Yin, Sheng Dai, and Shouheng Sun. A general approach to noble metal- metal oxide dumbbell nanoparticles and their catalytic application for co oxidation. *Chemistry of Materials*, 22(10):3277–3282, 2010.

[66] Yuanpeng Wu, Fang Zuo, Zhaohui Zheng, Xiaobin Ding, and Yuxing Peng. A novel approach to molecular recognition surface of magnetic nanoparticles based on host–guest effect. *Nanoscale research letters*, 4(7):738, 2009.

[67] Chao Wang and Chenxu Yu. Detection of chemical pollutants in water using gold nanoparticles as sensors: a review. *Reviews in Analytical Chemistry*, 32(1):1–14, 2013.

[68] Guozong Yue, Song Su, Na Li, Maobing Shuai, Xinchun Lai, Didier Astruc, and Pengxiang Zhao. Gold nanoparticles as sensors in the colorimetric and fluorescence detection of chemical warfare agents. *Coordination Chemistry Reviews*, 311:75–84, 2016.

[69] A Sugunan, C Thanachayanont, Joydeep Dutta, and JG Hilborn. Heavy-metal ion sensors using chitosan-capped gold nanoparticles. *Science and Technology of Advanced Materials*, 6(3):335–340, 2005.

[70] Juewen Liu and Yi Lu. Preparation of aptamer-linked gold nanoparticle purple aggregates for colorimetric sensing of analytes. *Nature protocols*, 1(1):246, 2006.

[71] Jin Liu, Michael Svard, and Åke C Rasmuson. Influence of agitation on primary nucleation in stirred tank crystallizers. *Crystal Growth & Design*, 15(9):4177–4184, 2015.

# Appendix

## A PEG coated Au NS

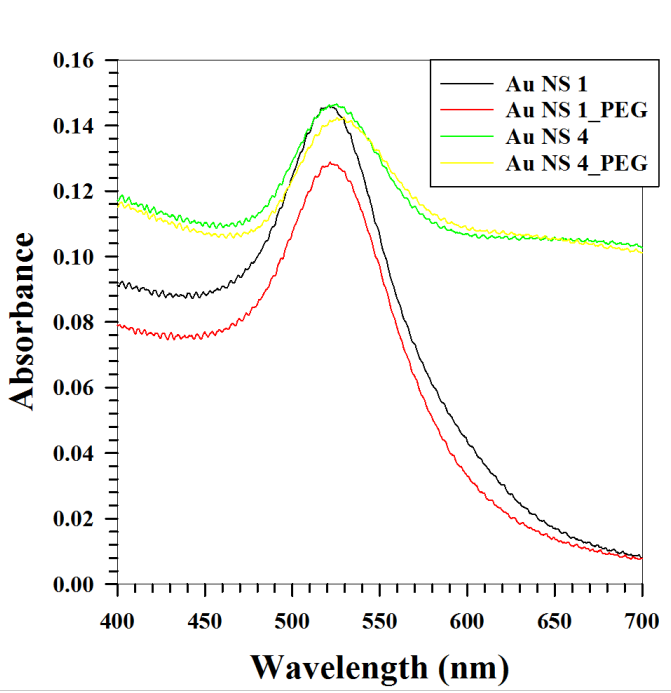


**Figure 5.1:** UV Vis spectra obtained for Au NS 1 and 4, PEG coated Au NS 1 and 4

# B Sample VPTT calculation

Calculations to find VPTT of NG_C is shown here.

The actual sizes of measured were converted in to swelling ratio. A sample calculation or heating cycle is given in Table 5.1

| Temperature (°)C | Size (nm) | Swelling ratio |
|---|---|---|
| 25 | 214.8 | 1 |
| 30 | 206 | 0.89 |
| 35 | 173 | 0.51 |
| 40 | 89 | 0.072 |
| 45 | 86 | 0.065 |
| 50 | 86 | 0.064 |
| 55 | 85 | 0.063 |

**Table 5.1:** Calculation of swelling ratio from size

Triplicate measurements of such heating and cooling cycles were plotted as shown in Figure 5.2

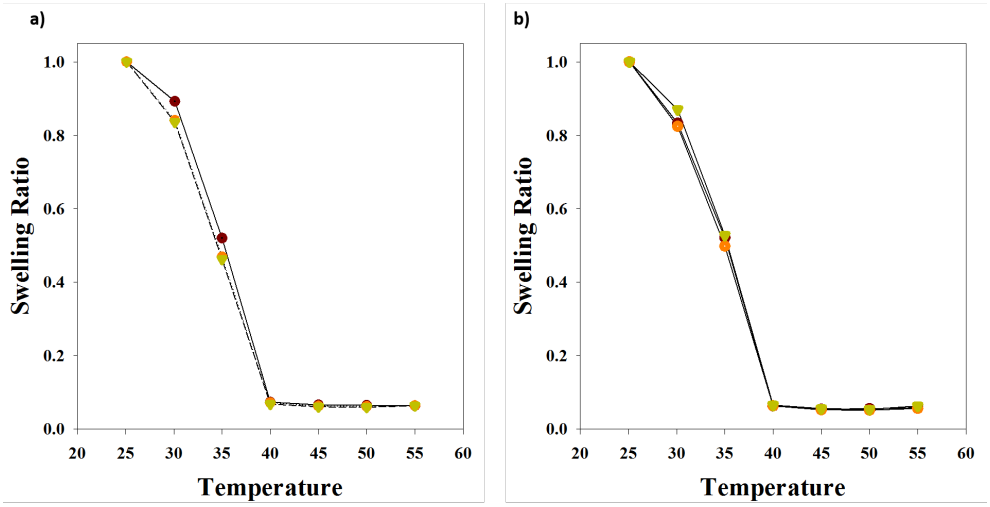


**Figure 5.2:** a) Heating cycle b) cooling cycle of NG_Continuous

Sigmoidal 5 paramemter fit was used on these curves to generate coefficients. Table5.2 shows the coefficient obtained for the curve obtained from Table 5.1.

| Coefficient | Value |
|---|---|
| a | 0.9583 |
| b | -2.9221 |
| c | 20441.5668 |
| x0 | 64.86 |
| y0 | 0.0629 |

**Table 5.2:** Coefficients obtained after curve fit

Similar procedure was followed for the cooling curve. These coefficients were given to the MatLab code and the VPTT was found as 36.4°C. Average VPTTs and standard deviations were found from three such measurements.

# C Time based study graphs

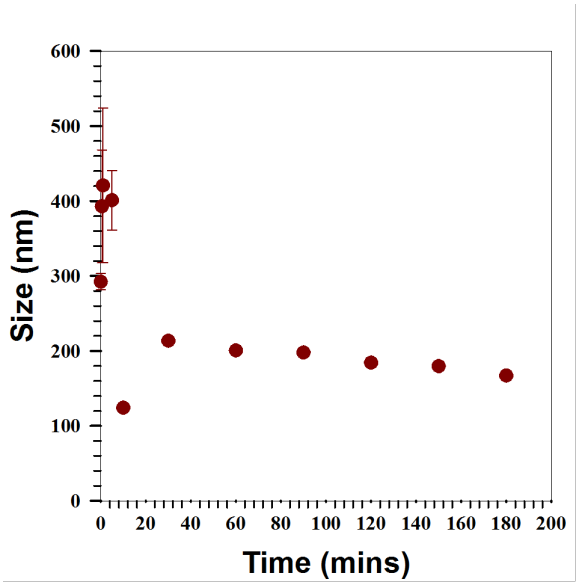


**Figure 5.3:** Size vs Temperature measurements for NG_Continuous

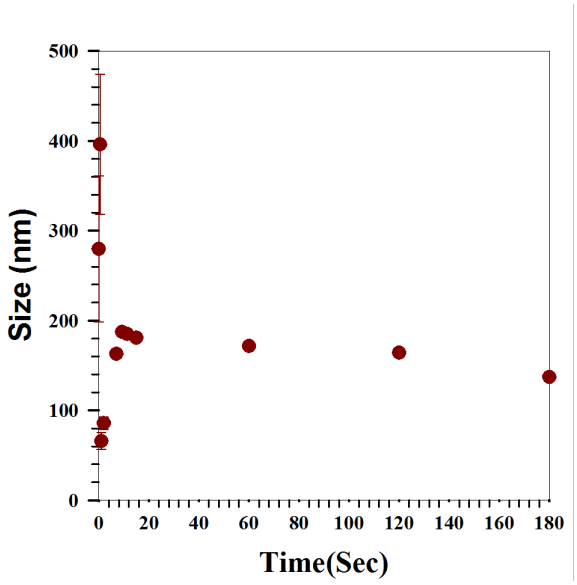


**Figure 5.4:** Size vs Temperature measurements for NG_lashing

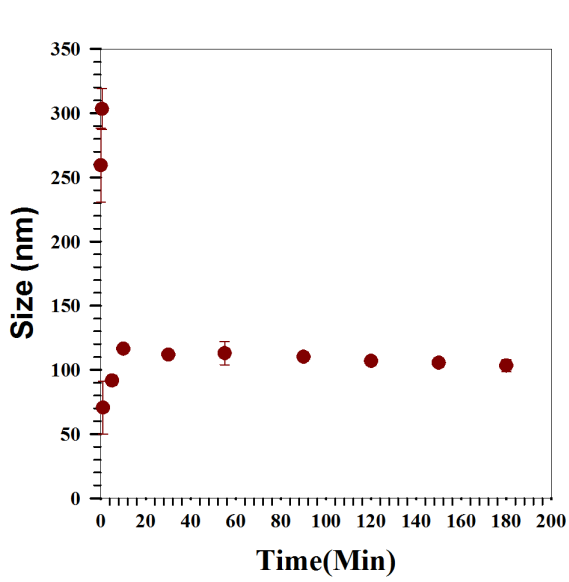


**Figure 5.5:** Size vs Temperature measurements for NG_Impeller

# D Curve fitting of Normalized size vs time

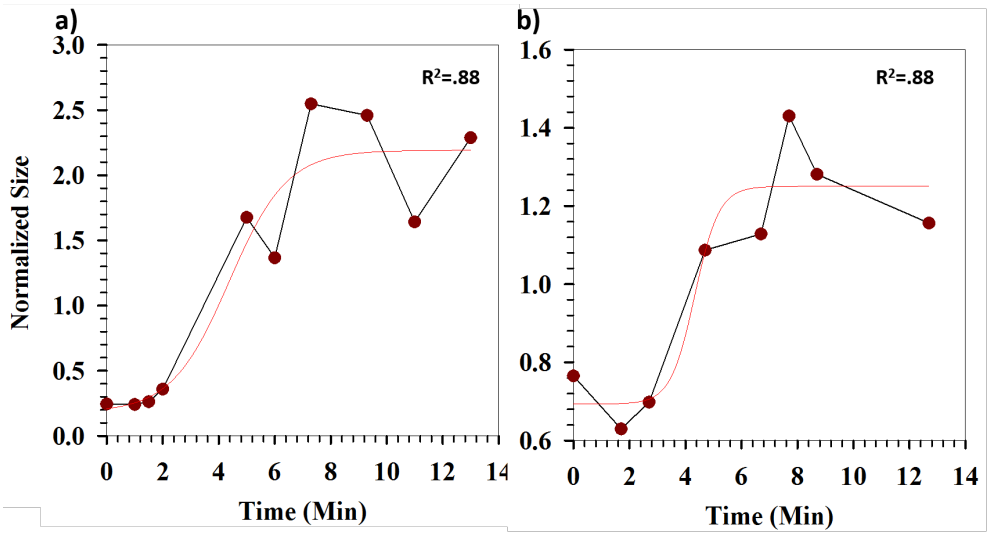


**Figure 5.6:** Curve fit for Normalized size vs time for a)NG_Flashing b)NG_Impeller

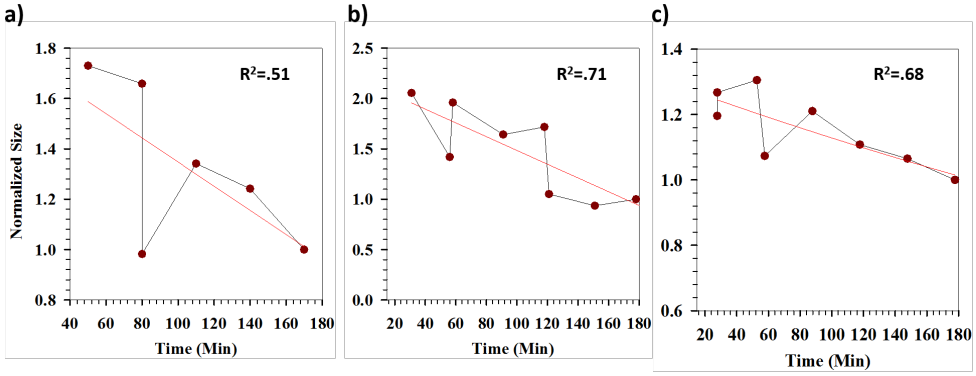


**Figure 5.7:** Curve fit for Normalized size vs time for a)NG_Continuous b)NG_Flashing c)NG_Impeller

# E VPTT Graphs

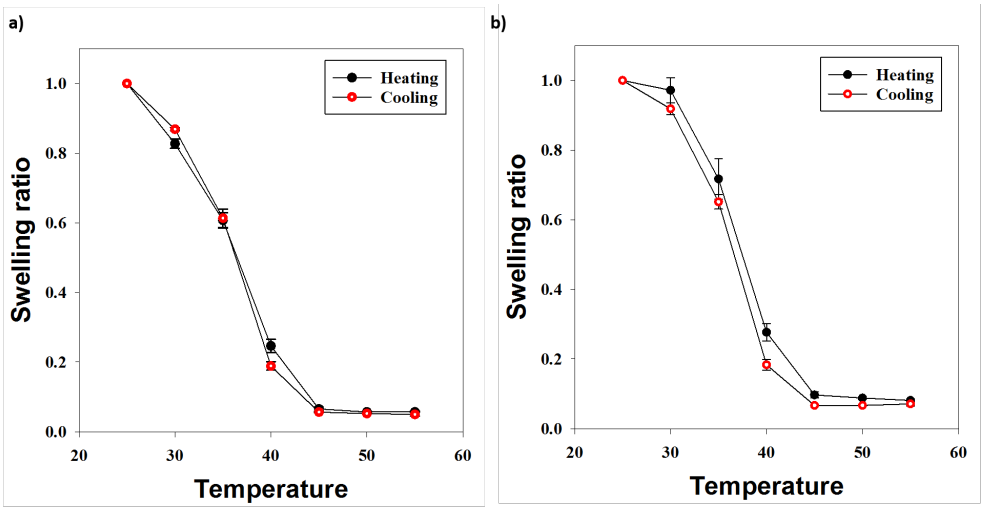


**Figure 5.8:** VPTT graphs of a) NG_Flashing b)NG_Impeller

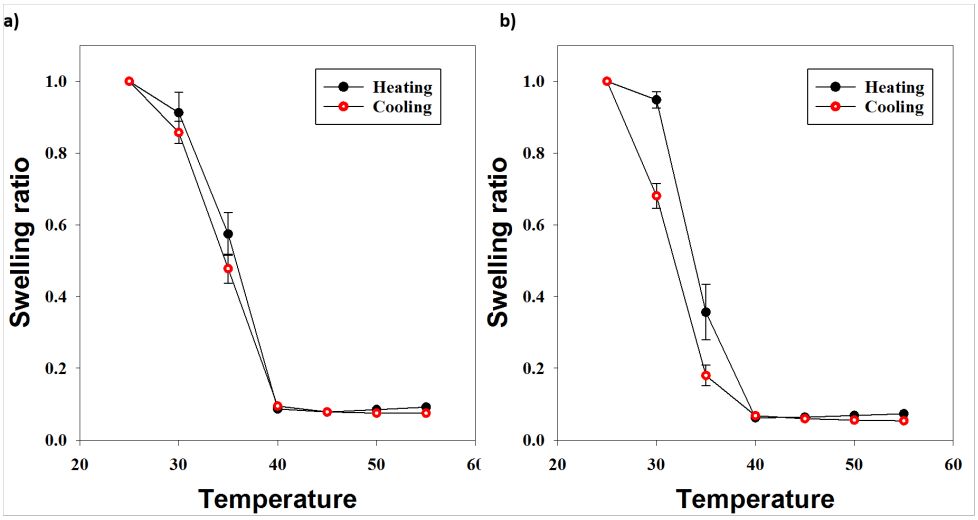


**Figure 5.9:** VPTT graphs of a) Au NS1_NG b)Au NS4_NG

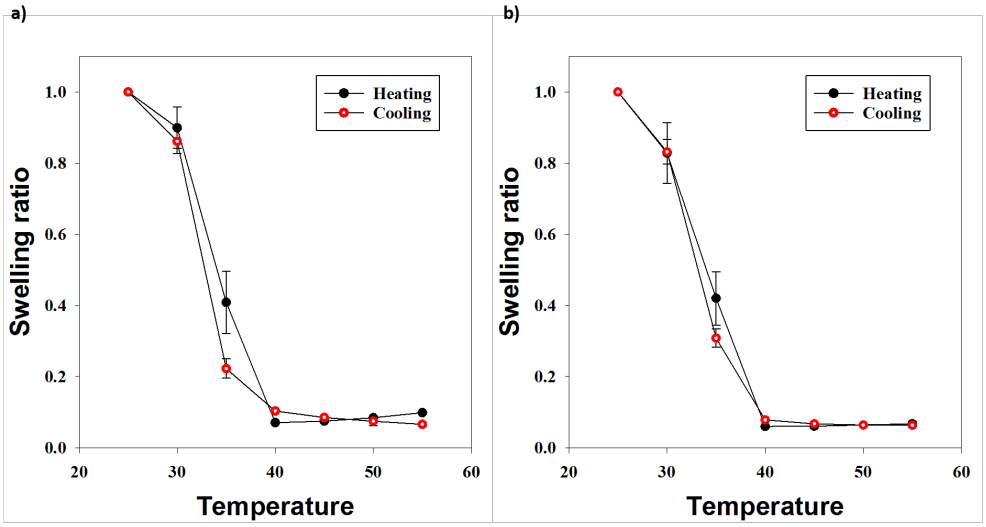


**Figure 5.10:** VPTT graphs of a) Fe_Flashing_NG b)Fe_Impeller_NG

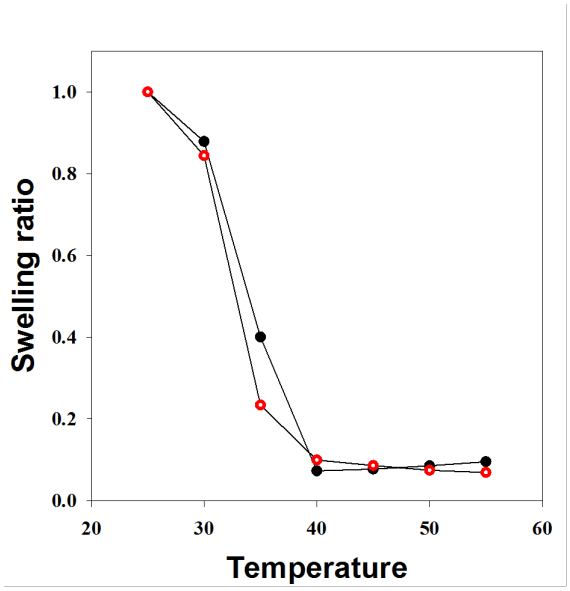


**Figure 5.11:** VPTT graphs of EtchedRod_NG

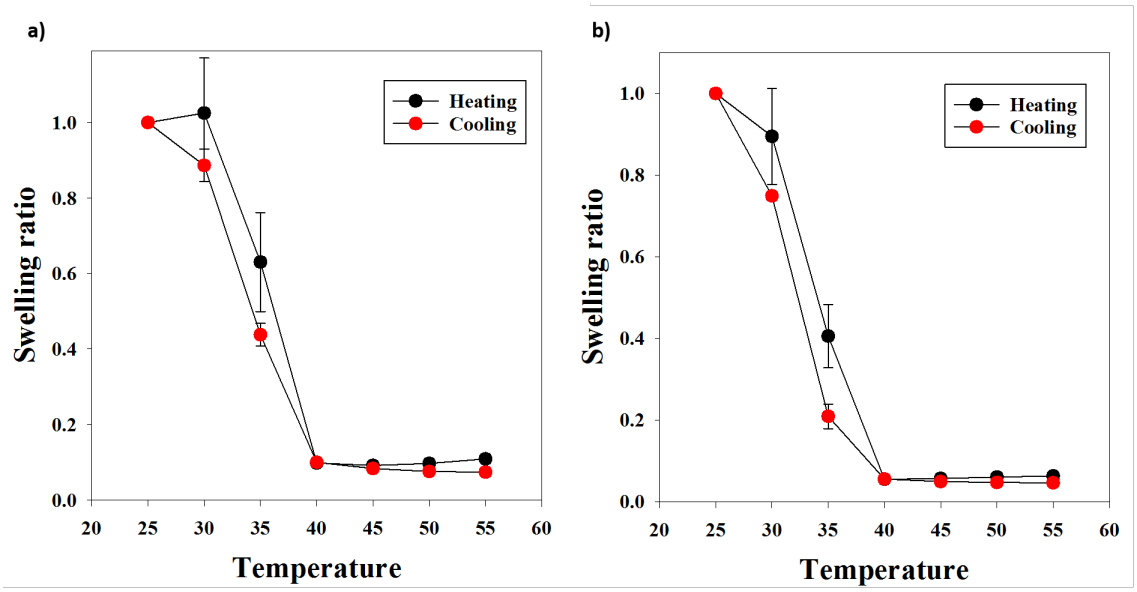


**Figure 5.12:** VPTT graphs of a)Au NS1_PEG_NG b)Au NS4_PEG_NG

# F UV-Vis spectra of hybrid NPs

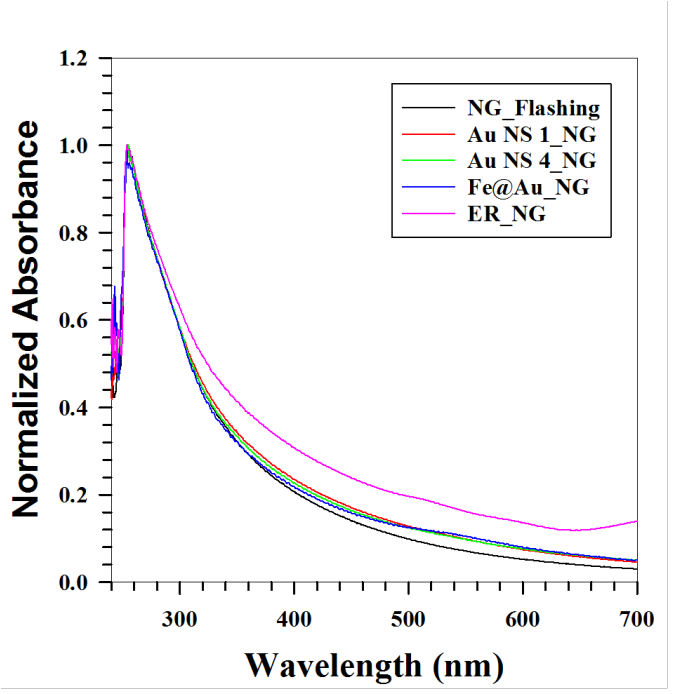


**Figure 5.13:** Representative graph containing UV-Vis spectra of hybrid NGs